Afdelingen for Bærende Konstruktioner
Department of Structural Engineering
Danmarks Tekniske Højskole · Technical University of Denmark

Uniaxial Stress-Strain Curves for Normal and High Strength Concrete

Kaare K.B. Dahl

Serie R No 282 1992

KAARE K.B. DAHL.

Uniaxial Stress-Strain Curves for Normal and High Strength Concrete

Kaare K. B. Dahl

Uniaxial Stress-Strain Curves for Normal and High Strength Concrete

Tryk:
Afdelingen for Bærende Konstruktioner
Danmarks Tekniske Højskole
Lyngby
ISBN 87-7740-097-6

Preface

This report has been prepared as a part of the investigations concerning high strength concrete. The investigation is part of the structural research program 'High Performance Concretes in the 90'ies'.

The work has been carried out at the Department of Structural Engineering, Technical University of Denmark, under the supervision of Professor, Dr.techn. M. P. Nielsen.

I wish to express my sincere thanks to my supervisor and the entire staff at the Department for their help during the time I have worked here.

Finally I gratefully acknowledge the financial support granted by the structural research program 'High Performance Concretes in the 90'ies', which in turn is financed by the Danish Industri- og Handelsstyrelsen.

Frederiksberg, 1992

Kaare K. B. Dahl

Summary

This report describes the test rig used, and the results obtained, in a large investigation concerning the complete uniaxial stress-strain curves for concrete. The work is centered on the complete stress-strain curve for concrete in the range 10 to 110 MPa.

For this range of concrete strengths the following properties have been studied: the E-modulus, the E-modulus at 45% load, the strain at peak load, and the complete stress-strain curve for strains below 6‰. It was found that the prediction of the E-modulus, as given by the CEB model code, [90.1], leads to acceptable results. It was also found that the strain at peak load is not constant, as stated by the CEB model, but is very much depending on the aggregates. If the formula for the strain at peak load is changed, the CEB model leads to acceptable results.

Also studied were the crack system, and the crack propagation, on both the ascending and the descending part of the stress-strain curve. The cracks were studied by making a number of polished sections on a normal and a high strength concrete. Prior to making the polished sections the concrete specimens were subject to a strain varying between 1 and 6‰.

The polished sections showed that the cracking of concrete mainly takes place after the peak load has been reached, and that only few microcracks appear in the concrete prior to the peak load.

Resumé

Denne rapport beskriver forsøgsopstillingen, samt de opnåede resultater, i et stort forsøgsprogram omhandlende den komplette eenaksede arbejdskurve for beton. De undersøgte betoner varierede i styrke fra 10 til 110 MPa.

For denne variation af den eenaksede betonstyrke er følgende undersøgt: begyndelses E-modulet, tangent E-modulet ved 45% last, tøjningen ved maksimal last, samt den komplette eenaksede arbejdskurve for tøjninger mindre end 6‰. Det blev fundet, at E-modulet ikke afviger meget fra den af CEB model code 90 forudsagte værdi. Det blev ligeledes fundet, at tøjningen ved maksimal last ikke er konstant, således som det er forudsagt i CEB model code, men i stedet er meget afhængig af tilslaget. Hvis formlen for tøjningen ved maksimal last ændres, giver CEB model code brugbare resultater.

Udover ovennævnte blev også revnesystemet i betonen, samt dettes udbredelse studeret på både den opadgående og den nedadgående del af arbejdskurven. Dette blev gjort ved at studere planslibninger hidrørende fra beton, der havde været udsat for tøjninger på mellem 1 og 6‰.

Planslibningerne viste, at revnedannelse sker efter toppunktet på arbejdskurven. Der sker således ingen revnedannelse, bortset fra dannelsen af enkelte mikrorevner, på den opadgående del af arbejdskurven.

List of contents

Notation

In this report standardized SI units and European symbols have been used. Any deviations from this are described in the text when they occur.

A_{center}	Area of the center steel cylinder.
A_c	Area of the concrete cylinder.
D_{actual}	Actual deformation of the distance between the top and bottom plate of the hydraulic jack.
D_{bridge}	Average deformation of the steel columns.
E_{c0}	Young's modulus at the origin (ϵ_c=0).
E_{c45}	Secant modulus for σ_c=0.45f_c.
E_{peak}	Secant modulus (f_c/ϵ_c).
E_{center}	E-modulus for the center steel cylinder.
f_c	Uniaxial concrete strength.
GF	Gauge factor; 2.02 for gauges placed on steel, 2.27 for gauges placed on concrete.
K_0	Ratio between D_{actual} and D_{bridge}.
K_a	K_0-factor, modified to include the influence of σ_c.
$K_{1000ton}$	Calibration factor, hydraulic jack.
k	Parameter in Tomaszewicz model.
L_c	Length of the concrete specimen.
L_{center}	Length of the center steel cylinder.
L_{col}	Length of the 4 steel columns.
n	Parameter in Tomaszewicz model.
V_{gauge}	Data signal form the gauge, single or full bridge.
V_{bridge}	Bridge excitation.
V_r	Datasignal.
w	Crack width.

σ	Stress.
σ_c	Stress in the concrete.
ϵ	Strain.
ϵ_c	Strain in the concrete.
$\epsilon_{c,max}$	Concrete strain on descending part of stress-strain curve where $\sigma_c=0.5f_c$
$\epsilon_{ccenter}$	Strain in the center steel cylinder.
ϵ_{col}	Strain in one of the 4 steel columns.
ϵ_{gauge}	Strain meassured by a concrete strain gauge.
ϵ_{peak}	Concrete strain at maximum stress ($\sigma_c=f_c$).
ν	Poisson ratio.

Chapter 1

Introduction

In the recent years high strength, or high performance, concrete has become more and more popular. The reason for its popularity is the greater demands of strength and durability that has been set by the engineers. However, high strength concrete is not just another concrete. In some ways it is a completely new material.

Therefore, a great need exists for investigating this new material prior to its use in everyday construction. In many cases is it not enough to extrapolate existing codes in order to include the higher strength concretes.

One of the simplest, and yet demanding, problems concerning concrete, is the complete uniaxial stress-strain behavior. Comparing low strength concrete to high strength concrete, one sees a dramatic change in the stress-strain behavior. In many ways can a low strength concrete be viewed as a perfect plastic material, whereas high strength concrete very much resembles a perfect elastic material.

Small changes in the material parameters, such as the E-modulus or the strain at peak load, will have only a marginal influence on the shape and area under the stress-strain curve of a low strength concrete. On a high strength concrete, however, small changes in these parameters bring a dramatic change in the stress-strain curve.

One of the reasons for this is the descending part of the stress-strain curve. In a low strength concrete, changing the peak strain will not have any significant effect, because the stress-strain curve is almost horizontal after peak load. In a high strength concrete, on the other hand, changing the peak strain will affect the area under the curve, as well as the center of gravity. This because the descending part of the stress-strain curves becomes steeper and steeper when increasing the concrete strength.

The use of high strength concrete therefore increases the need for a greater insight into the parameters that influence the stress-strain curve. Existing data show that i.e. the aggregate type has a large effect on the stress-strain curve. If high strength concrete is to be used safely it is therefore imperative that the effect of these parameters is better known.

A full scale investigation, such as the material research program 'High Performance Concrete of the 90'ies', naturally will include investigations into the stress-strain curve of concrete.

The goal of this investigation is therefore partly to see if some of the existing models can be extrapolated, with minor changes, to include high strength concrete, and partly to gather more information concerning the parameters influencing the stress-strain curve of concrete, as well as the fracture of concrete.

Chapter 2

Previous models

Throughout the years a number of models have been proposed to describe the uniaxial stress-strain relationship of concrete. In this chapter some of these models will be introduced.

2.1 The Tomaszewicz model

Tomaszewicz has in [84.1], as a part of a large Norwegian research program, reported an investigation concerning the uniaxial stress-strain relationship of normal and high strength concrete.

The proposed model has the form stated in (2.1)

$$\sigma = f_c \frac{\epsilon}{\epsilon_{peak}} \frac{n}{n - 1 + \left(\frac{\epsilon}{\epsilon_{peak}}\right)^{kn}} \tag{2.1}$$

where

- ϵ_{peak} : the strain at peak load
- E_{c0} : the E-modulus at $\epsilon=0$
- E_{peak} : f_c/ϵ_{peak}
- n : $E_{c0}/(E_{c0}-E_{peak})$
- k : a correction factor for the descending part (k=1 for $0<\epsilon<\epsilon_{peak}$)
- f_c : less than or equal to 85 MPa

and Youngs modulus, E_{c0}, is given by eq. (2.2).

$$E_{c0} = \frac{n}{n - 1} \frac{f_c}{\epsilon_{peak}} \tag{2.2}$$

With the proposed model only the 3 parameters, n, k, and ϵ_{peak}, need to be determined, in order for the stress-strain curve to be completely described.

On the basis of a limited number of test results, these parameters have been determined in [84.1]. However, instead of calibrating the model using n as a parameter, it is possible to calibrate using E_{c0} as a parameter. Doing so makes it possible to expand the model to include concretes with a uniaxial strength above 85 MPa. In eq. (2.3) such a calibration has been performed using the equation for E_{c0} given in the Norwegian Standard NS 3473.

$$E_{c0} = 10000 \cdot f_c^{0.3}$$

$$\epsilon_{peak} = \frac{0.7}{1000} \cdot f_c^{0.31} \qquad (2.3)$$

$$k = \frac{f_c}{20} \qquad \text{for } \epsilon > \epsilon_{peak}$$

The proposed model is of interest because it makes it possible to describe the complete stress-strain curve by means of one equation. However, the descending part of the stress-strain curve has proven to be very sensitive to the different parameters, which makes it troublesome to use in some cases.

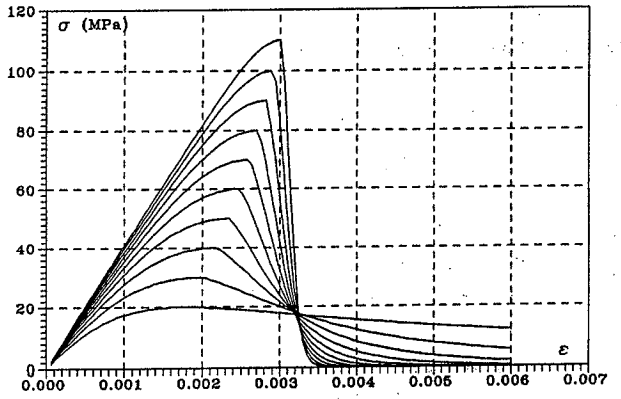

Fig. 2.1: Complete stress-strain curves, Tomaszewicz [84.1].

In Fig. 2.1 are shown the stress-strain curves for varying uniaxial concrete strength.

The model has some other points of interest, of which the following can be mentioned:

- the peak strain, ϵ_{peak}, is depending on the concrete strength, and reaches a maximum of ~3‰ for a 100 MPa concrete.
- the ascending part of the stress-strain curve is linear up to 70-75 % for the high strength concretes, and shows very little curvature near peak.

2.2 The CEB Model

The CEB model code 1990, [90.1], has suggested a σ-ϵ relationship as stated in eq. (2.4). This model covers strains in the range $0 \le \epsilon \le \epsilon_{c,max}$, where $\epsilon_{c,max}$ is given by eq. (2.5). For strains larger than $\epsilon_{c,max}$, the stress-strain curve is given by eq (2.6).

$$\sigma = f_c \cdot \frac{\frac{E_{c0}}{E_{peak}} \cdot \frac{\epsilon}{\epsilon_{peak}} - \left(\frac{\epsilon}{\epsilon_{peak}}\right)^2}{1 + \left(\frac{E_{c0}}{E_{peak}} - 2\right)\frac{\epsilon}{\epsilon_{peak}}} \qquad \text{for } \epsilon \le \epsilon_{c,max} \qquad (2.4)$$

where

$\epsilon_{peak} = 0.0022$

$E_{c0} = 21500\ (f_c/10)^{1/3}$

and the descending part of the stress-strain curve, given by eq. (2.4), is valid only for $\sigma/f_c \ge 0.5$. The strain $\epsilon_{c,max}$ corresponding to $\sigma = 0.5 f_c$ on the descending part of the stress-strain curve, can be found using eq. (2.4).

$$\frac{\epsilon_{c,max}}{\epsilon_{peak}} = \frac{1}{2}\left(\frac{1}{2}\frac{E_{c0}}{E_{peak}} + 1\right) + \sqrt{\frac{1}{4}\left(\frac{1}{2}\frac{E_{c0}}{E_{peak}} + 1\right)^2 - \frac{1}{2}} \qquad (2.5)$$

For strains larger than $\epsilon_{c,max}$ the descending part of the stress-strain curved may be described using (2.6).

$$\sigma = \frac{f_c}{\left(\frac{1}{\frac{\epsilon_{c,max}}{\epsilon_{peak}}} \cdot \xi - \frac{2}{\left(\frac{\epsilon_{c,max}}{\epsilon_{peak}}\right)^2}\right) \cdot \left(\frac{\epsilon}{\epsilon_{peak}}\right)^2 + \left(\frac{4}{\frac{\epsilon_{c,max}}{\epsilon_{peak}}} - \xi\right) \cdot \frac{\epsilon}{\epsilon_{peak}}} \qquad (2.6)$$

Where ξ is given by eq. (2.7).

$$\xi = \frac{4 \cdot \left(\left(\frac{\epsilon_{c,max}}{\epsilon_{peak}}\right)^2 \cdot \left(\frac{E_{c0}}{E_{peak}} - 2\right) + 2\frac{\epsilon_{c,max}}{\epsilon_{peak}} - \frac{E_{c0}}{E_{peak}}\right)}{\left(\frac{\epsilon_{c,max}}{\epsilon_{peak}} \cdot \left(\frac{E_{c0}}{E_{peak}} - 2\right) + 1\right)^2} \qquad (2.7)$$

The CEB model has some interesting points:

- The peak strain is independent of the uniaxial strength of the concrete.
- The stress-strain curve is almost linear in the ascending part, and show very little curvature near peak stress.
- It is possible to model the important part of the stress-strain curve, that is the ascending and some of the descending part, using only one equation.
- It is very simple to change the model to fit a certain concrete, due to the relatively insensitivity of the model to change in the E-modulus, and the peak strain.

However, there are also some factors where the model is not good enough:

- The model only yields useful stress-strain curves when $f_c \leq 90$ MPa. This because for the very high strength concretes does the model predict almost no post-peak behavior, in that the descending part of the stress-strain curve is almost vertical.
- When the concrete strength exceeds 102 MPa, the secant modulus, E_{peak} exceeds the tangent modulus E_0, which of cause cannot be true.

In Fig. 2.2 are shown the stress-strain curves for varying concrete strengths.

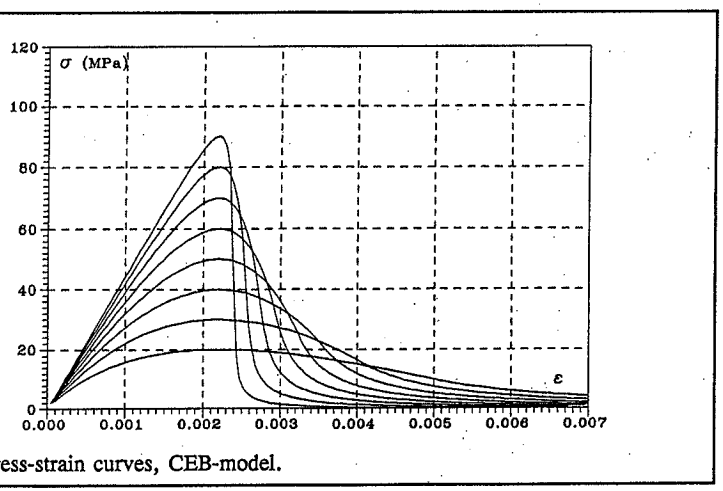

Fig. 2.2: Stress-strain curves, CEB-model.

2.3 The Exner model

Exner has proposed a model for the stress-strain curve in [83.1]. The model is based on the work of Wang, Shah and Naaman reported in [78.1]. The proposed equation is as stated in eq. (2.8).

$$Y = \frac{A \cdot X + B \cdot X^2}{1 + C \cdot X + D \cdot X^2} \qquad (2.8)$$

$$Y = \frac{\sigma}{f_c} \qquad X = \frac{\epsilon}{\epsilon_{peak}}$$

The stress-strain curve is described by two sets of constants for the equation (2.8). One set for the ascending part, and one set for the descending part. In order to determine the constants, some characteristic quantities of the stress-strain curve are used. The quantities are based on a regression analysis of the test results in [78.1]. In eq (2.9) are given the quantities used for the ascending part, and in eq (2.10) are given the quantities used for the descending part of the stress-strain curve.

Ascending part

$$\epsilon_{peak} = 0.00230 + 0.0000181 \cdot f_c$$

$$E_{c0} = 6740 + 271 \cdot f_c \qquad (2.9)$$

$$E_{c45} = E_{c0}$$

$$\frac{dY}{dX} = 0 \qquad \text{for } X = 1$$

Descending part

$$Y = \frac{13.96 + 0.085\, f_c}{f_c} \qquad \text{for } X = \frac{0.00802 + 0.000014\, f_c - \epsilon_{peak}}{\epsilon_{peak}}$$

$$\frac{dY}{dX} = 0 \qquad \text{for } X = 1 \qquad (2.10)$$

$$Y = 1 \qquad \text{for } X = 1$$

$$\lim_{X \to \infty} Y = 0$$

In order to produce a stress-strain curve for a given concrete, it is therefore necessary to find the 8 parameters in eq. (2.8). It is possible to determine a set of equations for the 8

parameters based solely on the concrete strength. However, these equations would not be very sensibly because of the rather large non-linearity between these parameters and the concrete strength. As an example would the best fit of the parameter B, on the ascending part, be a 6-degree polynomium in f_c.

The model has another property which makes it dubious. The problem is in the ascending part of the stress-strain curve. Using this model will result in the stress-strain curve getting an inflection point at about $0.2f_c$. This is best seen in the case of higher strength concretes, and when the peak strain is reduced. The infliction point on the ascending part of the stress-strain curve is an inherent property of eq. (2.8), and cannot be avoided.

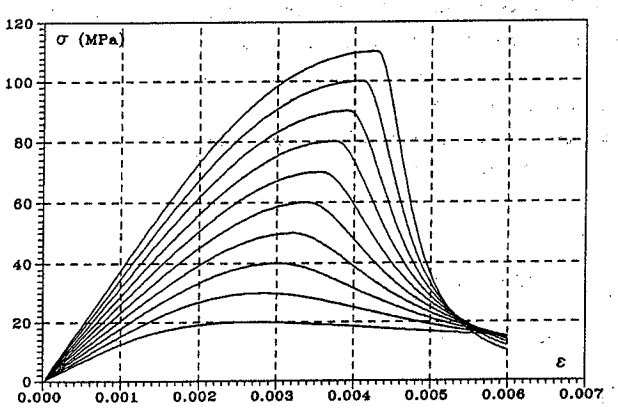

Fig. 2.3: Stress-strain curves for varying concrete strength, Exner model.

The interesting points of this model can be concluded as follows:

- The strain at peak stress is depending on the concrete strength.
- The descending part of the stress-strain curve is not as steep as previous mentioned models.

The dubious points of the model can also be concluded as follows:

- The ascending part is not linear up to 70-75% of f_c for higher concrete strengths, which is contrary to most other reported tests.
- The model fails to yield a simple way of determining the stress-strain curve for a given concrete.

- The strain at peak stress seems rather high, especially for the high strength concretes.
- The sign of the curvature of the stress-strain curve is not the same throughout the ascending part.

In Fig. 2.3 are shown the resulting stress-strain curves for different concrete strengths.

2.4 Summary

A summary of the general accepted properties of the stress-strain curve for concrete is hard to establish, since a lot of conflicting experimental evidence have been published. However, in the following an attempt in summarizing some of the properties of the stress-strain curve will be made.

Linearity

Most experimental evidence from high strength concrete tests show, that for concretes above ~60 MPa, the ascending part of the stress-strain curve is almost linear for stresses up to 70-75 % of the concrete strength.

E-modulus

It is generally accepted that the E-modulus for concrete increases for increasing strength. Many attempts have been made to formulate a relation between the concrete strength and the E-modulus. Since the E-modulus is depending on many other properties than the concrete strength, i.e. aggregate type and -content, such a relation will be, at the most, only a guideline. It seems, however, that the CEB-formula yields good results in estimating the E-modulus. Furthermore have an attempt been made in the CEB-formula, to incorporate the aggregate type in the determination of the E-modulus.

Strain at peak stress

The value of the concrete strain at peak stress seems to be a subject of much controversity. Some researchers are convinced that the peak strain is independent of the concrete strength. Whereas others have published results that show a heavily dependance of ϵ_{peak} with respect to the concrete strength.

It seems as if one possibility have been overlooked, namely the influence of the aggregate type, and the aggregate shape. Some evidence indicates, that using crushed coarse aggregate will result in larger peak strains, as compared to using rounded or

weathered aggregates. However, in almost all of the reported tests the peak strains lies in the range 2-3‰ for concretes with a strength below 100 MPa.

Descending part

No agreement on the shape of the descending part of the stress-strain curve have yet been reached. Much of the disagreement seems, however, to be ascribed to the specimen size along with the testing equipment used. Generally the only thing agreed upon is that the slope of the descending part of the stress-strain curve increases for increasing concrete strength.

Chapter 3

Test equipment

In this chapter the test equipment used in this investigation is described. Also presented is the calibration of the equipment. Lastly is presented the method used in determining the complete stress-strain curve of concrete from the data signals given by the test rig.

3.1 The test rig

Capturing the descending part of the stress-strain curve for concrete normally calls for a very stiff and very expensive servo hydraulic testing machine. However, it is possible to create a very stiff testing environment by other means than using a very expensive testing machine. Creating a stiff testing environment is achieved by increasing the stiffness of the test rig. This, however, calls for a hydraulic jack capable of generating a very large force.

In this investigation the inexpensive way of testing has been performed. The hydraulic jack used was capable of generating a force of 10 MN. The necessary stiffness was obtained by placing the concrete test cylinder, Ø100·200, on a massive steel cylinder surrounded by 4 steel columns. The 4 steel columns were then loaded along with the concrete specimen.

The test rig is shown in Fig. 3.1 and 3.2.

In order to find the stress-strain curve for a given concrete cylinder the following procedure has been used:

1/ The stress in the concrete cylinder was measured using strain gauges mounted on the center cylinder.
2/ On the ascending part of the stress-strain curve, the strain in the concrete cylinder was measured using 3 strain gauges, mounted in the center third of the concrete cylinder.
3/ After reaching the peak load, the strain gauges on the concrete cylinder were disregarded, and the strain in the concrete was calculated on basis of the

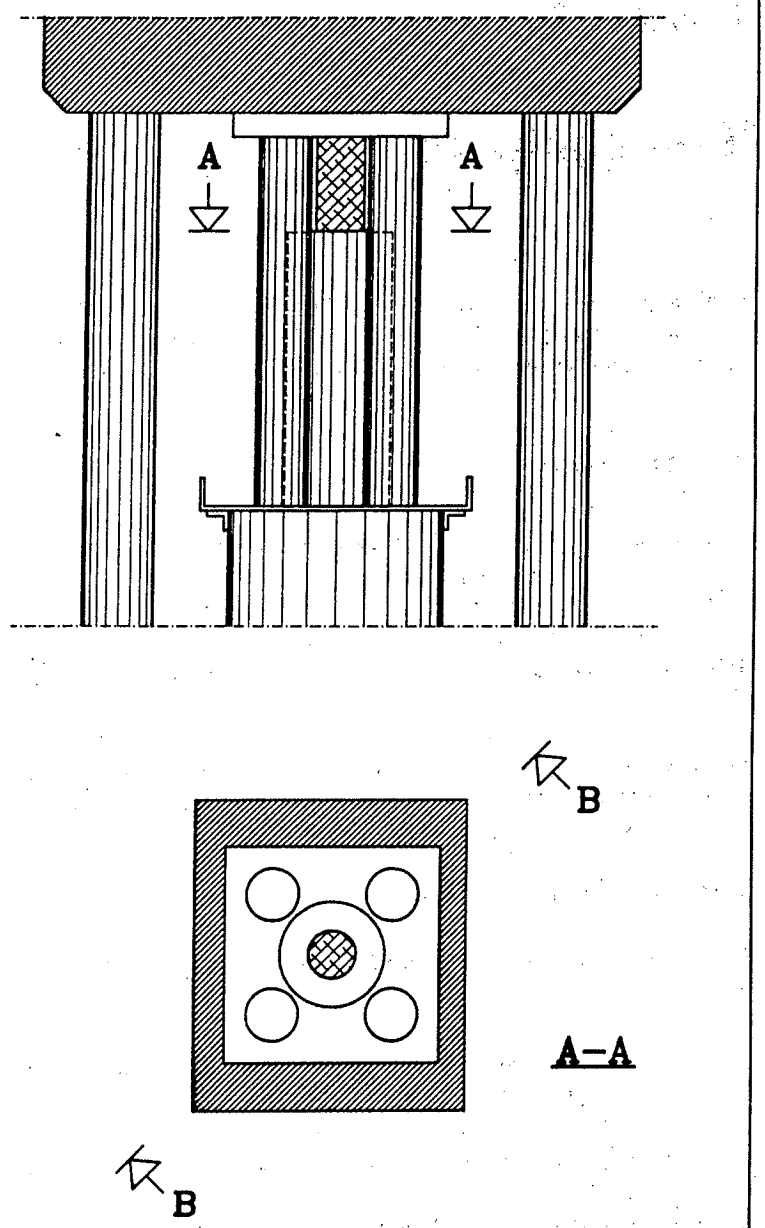

Fig. 3.1: The test rig.

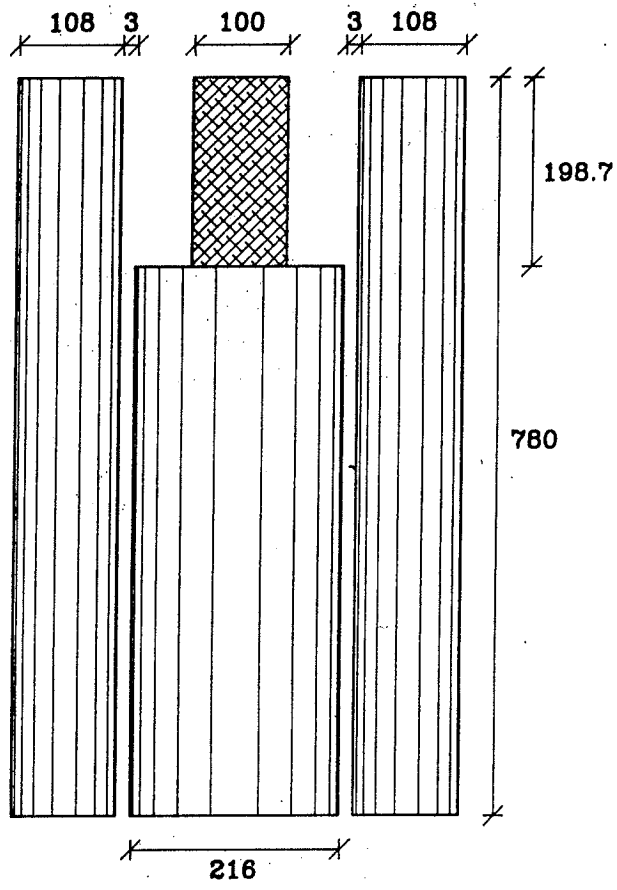

Fig. 3.2: Detail B-B of the test rig (all measurements in mm).

deformations of the 4 steel columns. The deformation of these columns was measured using strain gauges mounted at the middle of each of the columns.

Using this procedure for determining the stress-strain curve for concrete calls for a very thorough calibration of the test equipment. In the following chapter this calibration will be described.

3.2 Calibration of the test rig

3.2.1 Calibration of the 1000 tons hydraulic jack

The hydraulic jack used for generating the load was a Walter+Bai hydraulic jack, capable of supplying a force of 10 MN. The hydraulic jack was controlled by a servo unit also manufactured by Walter+Bai. It is possible by means of this servo unit to control, among other things, the load speed, the minimum load, the maximum load, and the error sensitivity of the jack.

The calibration was performed by applying a steadily increasing force from the hydraulic jack on a 1 MN load cell, and at the same time storing the signals supplied by both the servo controller and the load cell.

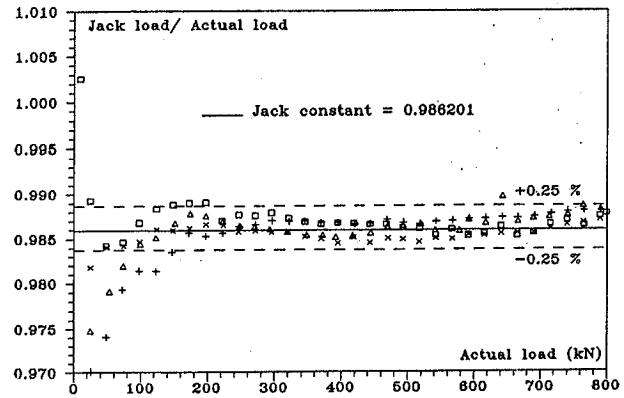

Fig. 3.3: Calibration result for 10 MN hydraulic jack.

The hydraulic jack was calibrated up to 800 kN. The calibration result is shown in Fig. 3.3, and the calibration constant was found to be as stated in eq. (3.1).

$$K_{1000ton} = 0.986201 \tag{3.1}$$

The calibration consisted of 4 loadings up to 800 kN. It can be seen in Fig. 3.3 that, apart from the region 0 to 100 kN, the calibration constant is very much linear, and with a very small deviation from the mean value. It can also be seen that for very small loads there is a large scatter in the results. This is a normal behavior for calibration test, and is due, among other things, to the internal friction in the jack, and to the numerical error normally experienced when working with small signals. This deviation is therefore disregarded when determining the calibration constant.

The hydraulic jack was used to supply a load up to 10 MN. It is therefore obvious that this calibration cannot be more than a guideline to show the deviation between the jack load and the real load. However, as can be seen in Fig. 3.3, there exist a very good correlation between the 2 signals. Therefore it was decided not to perform any further calibration test on the hydraulic jack, and instead use this calibration constant, (3.1), in the region 0 to 10 MN.

3.2.2 Calibration of the center steel cylinder

The center steel cylinder was used as a dynamometer for measuring the actual load on the concrete specimen. The measuring equipment consisted of 4 strain gauges mounted in a full bridge configuration, and placed at mid height of the steel cylinder. Using a full bridge eliminates the need for later compensation due to bending or temperature differences. The cylinder was calibrated up to 1000 kN, which is more than the maximum load the cylinder experienced during testing of the concrete. Prior to calibration the column was loaded and unloaded 10 times.

The calibration was performed 6 times, and data were collected at an interval of 100 kN. On the basis of these measurements the E-modulus for the steel has been calculated. In table 3.1 are given the result of the calibration.

	E-modulus (MPa)
test 1	212537
test 2	212077
test 3	211946
test 4	212011
test 5	211909
test 6	212053
mean value	212080
standard deviation	210

Table 3.1: Calibration result, center steel cylinder.

With such a small standard deviation in the results it is obvious that the mean value is very close to being the right one. The value E_{center}= 212080 has therefore been used in the subsequent calculations.

The strain in the center steel cylinder can then be calculated as stated in eq. (3.2)

$$V_r = \frac{V_{gauge}}{V_{bridge}} \text{(strained)} - \frac{V_{gauge}}{V_{bridge}} \text{(unstrained)} \qquad (3.2)$$

$$\epsilon_{center} = \frac{2\,V_r}{GF\,[(\nu + 1) - V_r\,(\nu - 1)]}$$

For ν a value of 0.3, corresponding to normal steel, has been used.

3.2.3 Calibration of the 4 steel columns

The 4 steel columns were used partly to increase the stiffness of the testing environment, and partly to measure the strain in the concrete on the descending part of the stress-strain curve (see also later). In order to measure the strain in the columns, 4 strain gauges were mounted in a full bridge configuration and placed at mid height of the columns. These full bridge strain gauge configurations were calibrated in the same way as the center cylinder. That is

they were centrically loaded with a maximum load of 3000 kN, and data were collected at an interval of 200 kN. Each column was loaded and unloaded 10 times prior to calibration, and calibration was performed 6 times.

The E-moduli for the columns were calculated on basis of these calibrations, and the result is stated in table 3.2.

	column 1 (MPa)	column 2 (MPa)	column 3 (MPa)	column 4 (MPa)
test 1	210591	210675	210454	209877
test 2	210430	210452	210440	209599
test 3	209937	210512	210239	209574
test 4	210060	210633	210399	209659
test 5	210380	210477	210265	209639
test 6	210069	210553	210339	209404
mean	210245	210550	210356	209626
standard deviation	257.7	88.2	89.9	151.3

Table 3.2: E-modulus for the 4 steel columns.

Since the deviation, both within each column, and between the columns, is very small it is then concluded that measuring the strain by means of this full bridge strain gauge configuration provides an excellent method of determining the average strain in the individual steel column.

In order to asses the strain distribution in the 4 steel columns during testing of the concrete, 18 strain gauges were mounted on 2 of the 4 columns. These single gauges were mounted at 6 positions along the columns. At each position, 3 gauges were mounted equidistant around the circumference of the column. A number of test runs were performed without having a concrete cylinder placed on the center steel cylinder. The later analysis of the collected data showed that the columns were not subjected to uniaxial compression, but were eccentrically loaded. Furthermore did the analysis reveal that the top and bottom loading plate of the hydraulic jack deformed during testing.

The reason turned out to be a lack of stiffness in the top and bottom loading plate. When

loaded, these plates deformed, and the head and foot of the steel columns then had to follow this angular displacement, causing the columns to bend. A careful study of this phenomena revealed that there existed a linear relation between the average deformations, as measured by the full bridge at the middle of the columns and the actual deformation of the distance between the top and bottom plate of the hydraulic jack. This relation is shown in Fig. 3.4, where the calculated deformation, based on the 18 single strain gauges is shown together with the average deformation given by the full bridge strain gauge configuration.

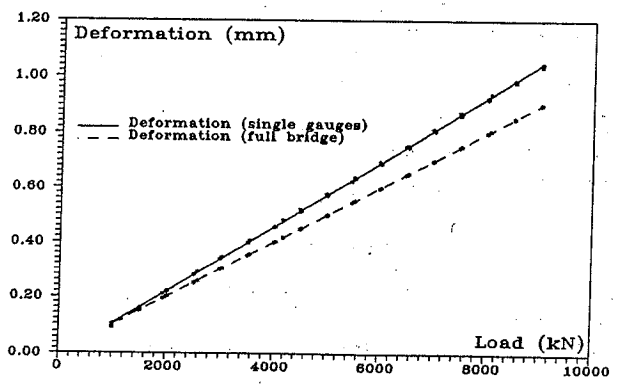

Fig. 3.4: Deformation calculated on the basis of the 18 single gauges, compared to the deformation given by the full bridge strain gauge configuration.

The ratio between the deformations given by the full bridge configuration, and the actual deformation has been found to be as stated in eq (3.3).

$$K_0 = \frac{D_{actual}}{D_{bridge}} = 1.1585 \tag{3.3}$$

The above mentioned test were performed without a concrete specimen on the center cylinder. It is obvious that loading a concrete cylinder along with the test rig will have a stiffening influence on the top and bottom plates of the hydraulic jack. The deformations will therefore be smaller when a concrete specimen is present in the test rig. A careful study of the later tests revealed that a linear relation existed between K_0 and the stress in the concrete cylinder, and that this relation approached unity for stresses equal to 70 MPa. On the basis of this the following formula for the factor K_a has been adopted (eq. (3.4)).

$$K_a = \begin{cases} 1 + (K_0 - 1) \cdot \dfrac{70 - \sigma_c}{70} & \text{for } \sigma_c \le 70 \text{ MPa} \\ 1 & \text{for } \sigma_c > 70 \text{ MPa} \end{cases} \tag{3.4}$$

3.3 Calculating the stress-strain curve

The resulting stress-strain curve for a given test is calculated in the following way. The actual stress in the concrete cylinder is given by converting the signal from the center steel cylinder to a corresponding strain, as described in chapter 3.2.1. This strain is then converted to a corresponding stress in the concrete specimen using eq. (3.6).

The strain in the concrete is calculated in two parts. On the ascending part of the stress-strain curve the strain is given as the average of the 3 gauges placed in the middle third of the concrete specimen. The signal from each one of these gauges is converted to a strain reading using eq. (3.5).

$$\epsilon = \frac{4\ V_r}{GF\ (1 + 2\ V_r)} \tag{3.5}$$

where V_r is calculated as in eq (3.2). The actual strain in the concrete is then given as stated in eq. (3.7). The ascending part of the stress-strain curve is defined as being prior to the point where the signal from the center steel cylinder starts decreasing.

On the descending part of the stress-strain curve the strain in the concrete cannot be calculated on basis of the concrete gauges, due to the severe cracking of the concrete which destroys these gauges. The strain is therefore calculated using the strains from all the 4 steel columns and the center steel cylinder. However, since the concrete and the 4 steel columns are not exactly of equal heights they will not have strained equally much. Therefore the following procedure has been adopted.

The strain **increment** of the 4 steel columns and the center steel cylinder is calculated. The strain increment is defined as the strain in the steel at the time when the peak load occurred in the concrete specimen, subtracted from the strain in the steel at the time considered. This value is added to the concrete strain also at peak loading, giving the actual concrete strain. The steel strains are calculated in the same way as for the center column, eq. (3.2). Using this procedure will result in the strains on the descending part of the stress-strain curve being

the average strains in the total concrete specimen. This is as opposed to the strains on the ascending part of the stress-strain curve, which are the average strains in the middle third of the concrete specimen.

Experimental evidence [64.1] has shown that under uniaxial loading the strains in the middle third of a concrete cylinder will be relatively unaffected of the friction between the concrete and the load plates. That is why the gauges on the concrete have been placed in the middle third. The discrepancy between the measuring of the strains on the ascending and the descending part of the stress-strain curve is unfortunate, but unavoidable. This due to the limitations of the gauges when placed directly on the concrete specimen.

The complete stress-strain curve is then calculated using eq. (3.6) to (3.8)

Stress, ascending and descending part

$$\sigma_c = E_{center}\,\epsilon_{center}\,\frac{A_{center}}{A_c} \tag{3.6}$$

Strain, ascending part

$$\epsilon_c = \frac{1}{3}\left(\epsilon_{gauge1} + \epsilon_{gauge2} + \epsilon_{gauge3}\right) \tag{3.7}$$

Strain, descending part

$$\epsilon_c = \frac{\left[\frac{1}{4}\left(\Delta\epsilon_{col1} + \Delta\epsilon_{col2} + \Delta\epsilon_{col3} + \Delta\epsilon_{col4}\right) K_a\right] L_{col} - \Delta\epsilon_{center} L_{center}}{L_c} + \epsilon_{peak} \tag{3.8}$$

Chapter 4

Experimental program

Described in this chapter are the test program and the mix design for the concretes used in the investigation.

4.1 The scope of the investigation

The scope of this investigation has been twofold. The first objective of the investigation has been to find the complete uniaxial stress-strain curves for concrete. The concrete strength was to be varied between 10 and 110 MPa, in order to include high strength concrete. The second objective has been to study the crack form, and the crack propagation in normal and high strength concrete, including the development of the cracks in the post peak region.

The first objective has been investigated by testing 9 different concretes with the uniaxial strength varying from 14 to 116 MPa. Furthermore has the influence of the aggregates been briefly studied by testing cement paste and 2 different mortars with varying aggregate content. The testing of the cylinders were performed under a constant deformation speed of ~13 micro strain/second.

The second objective has been studied by testing a normal strength concrete, f_c=22 MPa (E2), and a high strength concrete f_c=72 MPa (E6). A total of 6 cylinders from each concrete were tested. Each of the cylinders was tested using the test rig described in chapter 3. The test of the individual cylinder was stopped when the concrete was subject to a certain strain. The cylinders were subject to a strain of ~1‰, ~2‰, ~4‰, ~5‰, ~6‰, and at peak load. After unloading, the cylinders were impregnated by a fluorescent epoxy resin. After sufficient hardening of the epoxy, the cylinders were cut axially into two halves. One of the halves were then polished in order to make the crack system visible and ready for studying.

4.2 Description of the concrete

In the following chapter the materials, the mix proportions, the handling of the concrete, and the test specimens will be described.

4.2.1 Materials

The materials used have the following characteristics:

Binders:

Rapid hardening cement	ASTM type III, Danish classification PC(R).
White cement	A white, rapid hardening, low-alkali cement, ASTM type III or IV, Danish classification PC(R/L/S/H).
Low-alkali cement	ASTM type IV or V, Danish classification PC(A/L/S).
Fly Ash	Fly ash was supplied by Amagerværket, Copenhagen. Specific gravity was assumed to be 2200 kg/m^3.
Micro silica slurry	A solution of micro silica, with a dry-matter percentage of 51.6, and a density of 1391 kg/m^3.

Aggregate:

Sand	Danish marine deposits (0-4 mm), free of calcium chloride, with a specific gravity of 2567 kg/m^3.
Gravelit	Danish marine deposits (4-8 mm), free of calcium chloride, with a specific gravity of 2627 kg/m^3. Gravelit consists of small rounded pebbles, free of flint and lime.
Granite	Crushed Danish granite (4-16 mm), with a specific gravity of 2735 kg/m^3. The crushed granite had an oblong particle shape.

Admixtures:

Plasticizer	As plasticizer a product called CONPLAST 212 was used. CONPLAST 212 is a LIGNOSULFONAT based plasticizer, supplied by 4K-Byggeteknik A/S. CONPLAST 212 has a density of 1170 kg/m^3, and a dry-matter percentage of 36.
Super-plasticizer	As super-plasticizer a product called PERAMIN F was used. PERAMIN F is a MELAMIN based super-plasticizer supplied by 4K Byggeteknik A/S. PERAMIN F has a density of 1210 kg/m^3, and a dry-matter percentage of 34.

The water used was ordinary tap water from the city's network.

4.2.2 Mix proportions

9 different concrete mixes were used to produce the 9 different strength levels desired. Furthermore 2 different mortars, and 1 cement paste were produced.

The mix design for the paste and the mortars was determined simply by removing one or more of the aggregate fractions from one of the 9 concretes used. Hereby it was ensured that the uniaxial strength of the mortars, paste, and the concrete was approximately the same.

The mix design for mortar 2, M2, was established by removing all of the crushed granite from the mix design of the concrete E6. The mix design for mortar 1, M1, was established by removing all of the Gravelit from the mix design of mortar M2. Finally the mix design for the paste, P1, was established by removing all of the sand from the mix design of mortar M1.

The strengths of the concretes, mortars, and paste, varied from 14 to 116 MPa, as measured on Ø100·200 mm cylinders. In table 4.1 and 4.2 are given the mix proportions, and in table 4.3 the uniaxial compressive strength of the concretes and the mortars.

Concrete Material	E1	E2	E3	E4	E5	E6	E7	E8	E9
Cement (*)	129	180	172	247	260	309	320	375	390
Fly ash	69	75	69	100	40	-	45	-	-
MS-slurry	-	-	-	-	36	55	60	75	76
Water	170	170	158	170	150	129	95	70	63
Sand (0-4 mm)	754	618	640	618	600	598	610	615	521
Gravelit (4-8 mm)	246	244	272	244	257	265	186	188	247
Granite (4-16 mm)	985	977	1089	977	1026	1061	1106	1120	989
Conplast 212	-	-	-	-	1.4	2.0	2.0	2.3	2.4
Peramin F	-	-	-	-		3.1	6.3	8.3	12.0

Table 4.1: Mix proportions of the different concretes, used in the investigation. All units are kg/m³.

(*): The cement used was E7: low-alkali cement, E8: white cement, the remaining: rapid hardening cement.

Concrete Material	P1	M1	M2
Rapid Cement	1030	597	462
Fly ash	-	-	-
MS-slurry	183	106	82
Water	430	249	192
Sand (0-4 mm)	-	1156	904
Gravelit (4-8 mm)	-	-	395
Granite (4-16 mm)	-	-	-
Conplast 212	-	-	-
Peramin F	-	-	-

Table 4.2: Mix proportions of the paste, and the mortars, used in the investigation. All units are kg/m³.

4.2.3 Mixing, casting and curing

A 0.1 m³ paddle mixer was used to mix the concrete in batches of ~0.06 m³. The mixing procedure was as follows:

1/ The dry aggregates, sand and coarse aggregate, were mixed together in the paddle mixer for 5 minutes.
2/ The cement and fly ash were added, and mixing continued for 5 minutes.
3/ The water, micro silica slurry, plasticizer, and approx. 70% of the superplasticizer were blended together, and slowly added to the mixer. Mixing continued for 3 minutes.

4/ The concrete was examined, and if necessary more super-plasticizer was added until the fresh concrete had the desired workability.

Blending the fluids together prior to mixing has the advantages of, partly ensuring a better dispersal of the micro silica in the concrete, and partly of the plasticizers being more effective.

The slump was measured on the fresh concrete, prior to casting. The results are given in table 4.3.

The cylinders were cast in plastic moulds, and compacted on a vibrator table. The moulds were filled with 3 layers of concrete, with a thorough compaction between each layer.

After approximately 24 hours, the cylinders were removed from the moulds. The cylinders were then cured 13 days in water, and 14 days at 20°C and 60% RH. The paste cylinders varied from this, in that they were stored 24 days in water, and 3 days at 20°C and 60 % RH. The extra long water curing was performed in order to avoid shrinkage cracks in the paste. As the test results show, the shrinkage cracks were not avoided.

4.2.4 Uniaxial compressive strength

From each batch 6 Ø100·200 mm cylinders were tested in order to determine the uniaxial compressive strength of that particular batch. All the cylinders were tested in a 200 tons MP MFL compression jack controlled by a Walter+Bai servo controller.

The test cylinders for the standard strength tests were ground accurately plane by means of a diamond cutting spindle. Wood fiber plates were used between the steel loading platens and the concrete. Previous studies at the Department of Structural Engineering have shown these fiber plates to have no influence on the strength measurements. The cylinders were tested at a rate of 0.7 MPa/s, as specified by the Danish National Code, DS423 [84.2].

	Strength (MPa) test rig	std.dev. (%)	slump (mm)	Strength (MPa) standard
E1	14.41	3.22	100	14.75
E2	20.07	7.36	185	22.32
E3	31.00	3.50	80	32.32
E4	48.86	2.14	70	53.03
E5	64.86	1.32	80	66.37
E6	69.85	3.69	130	72.34
E7	96.77	4.37	70	93.10
E8	109.87	2.66	230	113.35
E9	114.48	5.00	200	112.34
P1	-	-	n.m.	43.97
M1	68.65	2.15	n.m.	73.17
M2	61.19	2.47	n.m.	65.97

Table 4.3: Slump and strength results of the concretes.
Note: The abbreviation, n.m., means not measured.

The paste cylinders failed due to the very severe shrinkage cracks that appeared shortly after the cylinders were removed from the water. The compressive strength shown here is therefore not the uniaxial compressive strength of the cement paste itself, but that of the shrink-cracked cement paste.

The test cylinders for the test rig were ground accurately plane by means of a diamond cutting spindle, and in the meanwhile the length was reduced from 200 mm to 198.7 mm, in order for the cylinders to fit in the test rig. The cylinders were tested at a rate of ~13 micro strain/second.

It is seen that there exists a good correlation between the uniaxial strength found in the test rig, and the uniaxial strength found in the standard strength test. It is also seen that the normal strength test generally yields a little higher strengths than in the test rig. This is most probably due to the lower loading speed used in the test rig, as compared to the standard test.

Chapter 5

Experimental results

In the following chapter the experimental results from the uniaxial compression test are presented. Also presented are the photographs of the crack systems in the concrete.

5.1 Uniaxial test data

The results of the uniaxial compression tests falls into two parts. The first part is the uniaxial stress-strain curve. These curves are presented in appendix 1. The second part is a number of characteristic quantities from each test. These quantities are the E-modulus at start, the E-modulus at 45% of peak load, the peak load, and the strain at peak load. In table 5.1 - 5.11 these data are given.

	f_c (MPa)	ϵ_{peak} (‰)	E_{c0} (MPa)	E_{c45} (MPa)
E1-1	13.68	3.463	18326.9	13640.3
E1-2	14.81	3.264	21816.1	15447.0
E1-3	14.81	2.923	23407.0	16638.8
E1-4	14.31	3.176	20600.1	15218.9
E1-5	14.44	3.297	19433.3	16322.8
E1-6	-	-	-	-
Mean value	14.41	3.224	20716.7	15453.6

Table 5.1: Results from uniaxial compression test, concrete E1.

	f_c (MPa)	ϵ_{peak} (‰)	E_{c0} (MPa)	E_{c45} (MPa)
E2-1	18.94	3.253	26855.5	20946.2
E2-2	20.45	-	-	-
E2-3	18.32	2.397	33393.8	25065.1
E2-4	21.96	2.798	25919.0	19691.0
E2-5	19.20	3.395	28019.4	21055.6
E2-6	21.52	2.669	24466.0	19053.0
Mean value	20.07	2.902	27730.7	21162.2

Table 5.2: Results from uniaxial compression test, concrete E2.

	f_c (MPa)	ϵ_{peak} (‰)	E_{c0} (MPa)	E_{c45} (MPa)
E3-1	30.97	3.390	29848.3	25716.9
E3-2	31.07	2.930	32830.8	25694.4
E3-3	28.91	2.704	27478.2	24322.8
E3-4	31.52	2.819	31502.7	26843.9
E3-5	31.90	3.301	29951.0	25170.5
E3-6	31.65	2.875	29319.4	25678.3
Mean value	31.00	3.003	30155.1	25571.1

Table 5.3: Results from uniaxial compression test, concrete E3.

	f_c (MPa)	ϵ_{peak} (‰)	E_{c0} (MPa)	E_{c45} (MPa)
E4-1	49.38	2.930	37759.6	30431.0
E4-2	47.75	2.735	34745.7	29901.1
E4-3	50.38	2.761	33046.0	30084.0
E4-4	49.24	2.772	34147.9	30556.1
E4-5	47.63	2.608	33890.2	30493.8
E4-6	48.78	2.636	34184.6	30352.7
Mean value	48.86	2.740	34629.0	30303.1

Table 5.4: Results from uniaxial compression test, concrete E4.

	f_c (MPa)	ϵ_{peak} (‰)	E_{c0} (MPa)	E_{c45} (MPa)
E5-1	64.78	2.610	35343.0	33641.8
E5-2	64.39	2.671	33993.6	32494.5
E5-3	63.46	2.511	37210.5	34123.7
E5-4	65.86	2.610	35394.9	33489.1
E5-5	65.21	2.718	34603.7	32924.2
E5-6	65.44	2.702	34764.5	32406.2
Mean value	64.86	2.637	35218.4	33179.9

Table 5.5: Results from uniaxial compression test, concrete E5.

	f_c (MPa)	ϵ_{peak} (‰)	E_{c0} (MPa)	E_{c45} (MPa)
E6-1	71.42	2.500	38184.3	35319.6
E6-2	73.77	2.539	37392.4	35602.3
E6-3	70.26	2.495	37658.5	35639.9
E6-4	68.90	2.642	34956.5	33820.4
E6-5	68.38	2.649	32512.0	32402.3
E6-6	66.37	2.568	37637.7	33533.5
Mean value	69.85	2.566	36390.2	34386.3

Table 5.6: Results from uniaxial compression test, concrete E6.

	f_c (MPa)	ϵ_{peak} (‰)	E_{c0} (MPa)	E_{c45} (MPa)
E7-1	91.89	2.578	41312.7	40416.3
E7-2	97.42	2.796	41948.8	41323.1
E7-3	103.08	2.951	41969.6	40695.6
E7-4	97.88	2.749	41073.7	41392.3
E7-5	94.23	2.708	40276.1	39941.5
E7-6	-	-	-	-
Mean value	96.90	2.756	41316.2	40753.8

Table 5.7: Results from uniaxial compression test, concrete E7.

	f_c (MPa)	ϵ_{peak} (‰)	E_{c0} (MPa)	E_{c45} (MPa)
E8-1	111.90	3.030	41611.0	41491.4
E8-2	113.82	3.109	41125.5	41583.2
E8-3	105.85	2.768	41622.5	41211.4
E8-4	110.01	2.910	41568.7	41294.2
E8-5	107.29	2.820	40742.0	40752.8
E8-6	110.33	2.960	41314.6	41372.7
Mean value	109.87	2.933	41330.7	41284.3

Table 5.8: Results from uniaxial compression test, concrete E8.

	f_c (MPa)	ϵ_{peak} (‰)	E_{c0} (MPa)	E_{c45} (MPa)
E9-1	116.66	3.092	43317.7	42237.8
E9-2	116.26	2.879	44385.3	43339.1
E9-3	103.76	2.675	44950.3	43176.4
E9-4	117.01	2.915	43327.4	42795.3
E9-5	120.19	3.177	43484.1	42745.8
E9-6	112.99	2.926	42688.9	42497.7
Mean value	114.48	2.944	43692.3	42797.0

Table 5.9: Results from uniaxial compression test, concrete E9.

	f_c (MPa)	ϵ_{peak} (‰)	E_{c0} (MPa)	E_{c45} (MPa)
M1-1	68.88	4.189	18651.1	21357.9
M1-2	68.71	4.165	18056.7	21074.2
M1-3	68.81	4.170	18617.5	21653.9
M1-4	66.19	3.847	19326.9	21417.5
M1-5	68.50	4.096	20097.6	21947.3
M1-6	70.83	4.243	20065.8	22120.0
Mean value	68.65	4.118	19135.9	21595.1

Table 5.10: Results from uniaxial compression test, mortar M1.

	f_c (MPa)	ϵ_{peak} (‰)	E_{c0} (MPa)	E_{c45} (MPa)
M2-1	59.93	2.786	26808.1	26517.6
M2-2	58.90	2.781	25571.6	26016.5
M2-3	62.58	2.970	25493.8	26254.7
M2-4	61.71	2.967	26840.8	26534.5
M2-5	61.27	2.765	27493.5	27621.0
M2-6	62.72	3.024	27655.8	27194.6
Mean value	61.19	2.882	26643.9	26689.8

Table 5.11: Results from uniaxial compression test, mortar M2.

As can be seen from table 5.10 and 5.11 the mortars generally have a lower E-modulus at start than at 45% of peak load. This might be a feature unique for mortars as compared to normal concretes, however unlikely that may be. It also might be due to the test rig, but no

further speculation on the cause of this behavior will be included in this investigation because of the rather small amount of data available.

As described earlier, tests have also been performed on cement paste. However, these cylinders had unfortunately not been cured under water for the whole period of 28 days. The air curing lead to many shrink cracks in the cylinders prior to testing, and the test results have therefore been disregarded. Although disregarded, the stress-strain curves are still given in appendix 1.

5.2 The stress-strain curves

In appendix 1 are given the stress-strain curves from this investigation. What follows here is a discussion of the capabilities of the test rig.

The stress-strain curves for the concretes E1-E6 are a series of smooth curves representing the actual stress-strain curve. When the concrete strength exceeded ~80 MPa the test rig was not stiff enough for capturing all of the descending part of the stress-strain curve. The stress-strain curves are still smooth up to, and a little past peak load. However, past peak load one of two things happened.

If the slope of the descending part was very steep, the concrete displayed an explosive failure, causing the test to stop. The explosive failure is due to the build-up of energy partly in the load plates, and partly in the center steel cylinder. If the slope is too steep the amount of energy released cannot quickly enough be transferred to the 4 steel columns, and explosive failure then occurs.

The alternative to an explosive failure is a partial failure. A partial failure is when the energy still cannot be transferred quickly enough to the 4 steel columns, but when the system recovers and the test can continue. The energy release is not as large as in the explosive failure, and it is small enough that the error sensitivity of the servo controller is not triggered causing abortion of the test. A partial failure can be seen in the stress-strain curves when they have a linear part in the descending branch.

The consequence of the lack of stiffness in the test rig is best seen in the tests of concrete E9. For this concrete all of the specimens exhibited explosive failures. Examples of partial failure can be seen in the tests of concrete E7, where some of the tests exhibited explosive failure causing abortion of the test just after peak load, and the rest of the tests exhibited partial failure.

5.3 Cracks in the concrete

In appendix 2 is given a number of photographs showing the crack systems, and their development, as the strain in the concrete is increased. A total of 12 concrete specimens were tested. The testing of these concrete cylinders was identical to the testing of the other concrete cylinders in this investigation, except when the stress in the cylinder reached a certain value, the test was stopped. In Fig. 5.1 and 5.2 is shown the location of the individual tests on a corresponding stress-strain curve.

It was intended that the cylinders were to be subject to a stress of 1/3, 2/3, and 3/3 f_c, on the ascending part of the stress-strain curve, and a stress of f_c-1/3(f_c-$\sigma_{0.006}$), f_c-2/3(f_c-$\sigma_{0.006}$), and f_c-3/3(f_c-$\sigma_{0.006}$), on the descending part, where $\sigma_{0.006}$ is the stress in the concrete at a strain of 0.006.

It was decided to use the stress, rather than the strain, as a stop criterion. This because if the strain was used as the stop criterion, then the polished sections number 4, 5, and 6 for concrete E6 would have been almost identical, due to rather large stress drop in the stress-strain curve after peak.

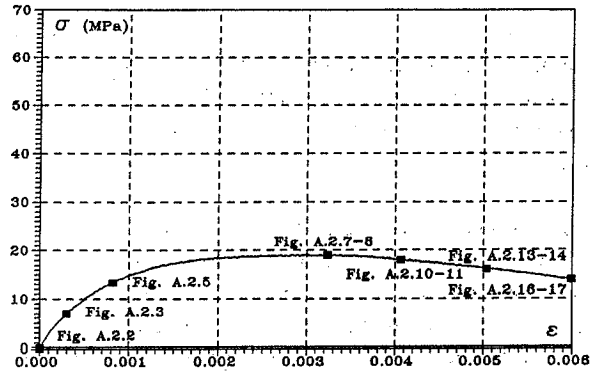

Fig. 5.1: Location of the individual polished sections on a corresponding stress-strain curve, concrete E2.

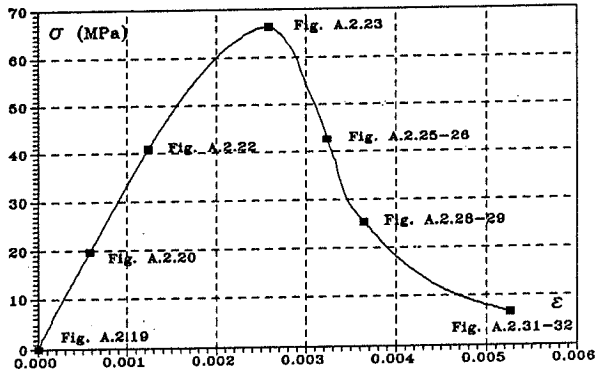

Fig. 5.2: Location of the individual polished sections on a corresponding stress-strain curve, concrete E6.

Chapter 6

Discussion of experimental results

In this chapter the results obtained in this investigation are evaluated, and compared to other reported experimental tests.

6.1 E-modulus

In Fig. 6.1 is shown the E-modulus from the tests in this investigation, compared to the CEB-model.

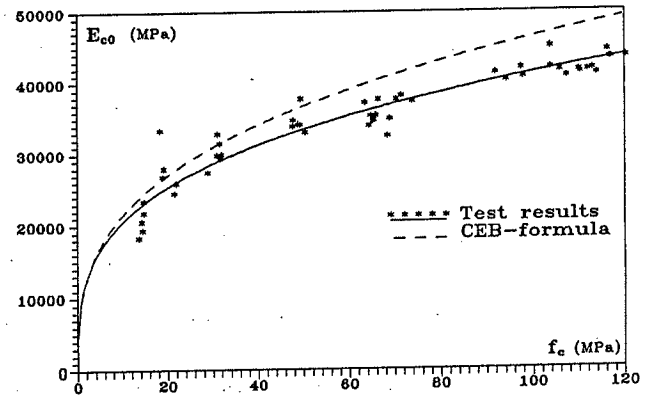

Fig. 6.1: E-modulus compared to the CEB-formula.

It is clearly seen that there exists a close resemblance between these test results, and the CEB-formula described in chapter 2.2. The difference between the test results and the CEB-formula is small for normal strength concrete. However, when the strength of the concrete is increased, the CEB-formula tends to predict a value of E_{c0} that is a little too high. The

overall picture, however, does not lead to a wish for changing the CEB-formula. This because it is known that the E-modulus is depending on many other parameters than the concrete strength. Changing the CEB-formula would therefore only lead to a better fit of the test data here presented, not a better understanding of the parameters influencing E_{c0}.

The best fit of the test results here presented is given in eq. (6.1).

$$E_{c0} = 10300 \cdot f_c^{0.3} \tag{6.1}$$

It is also seen that this formula represents very good the test results.

A global agreement exists on the linearity of the stress-strain curve, as explained in chapter 2.4. One way of describing this is to compare E-modulus at the origin, E_{c0}, with the secant E-modulus at $\sigma_c=0.45f_c$, E_{c45}. This is done in Fig. 6.2.

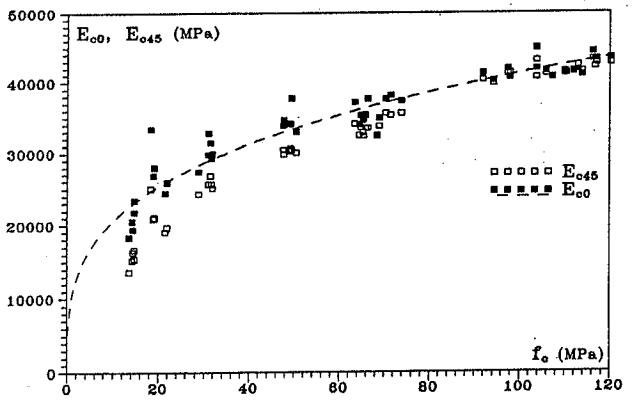

Fig. 6.2: E_{c0} compared with E_{c45}.

It is seen that E_{c45} approaches E_{c0} for increasing concrete strength. The corresponding stress-strain curve will then become more and more linear in the ascending part for increasing concrete strength.

6.2 Strain at peak stress

In Fig. 6.3 is shown the peak strain in the concrete specimens tested in this investigation. The peak strain is defined here as the strain in the concrete at the time when the stress in the concrete starts diminishing.

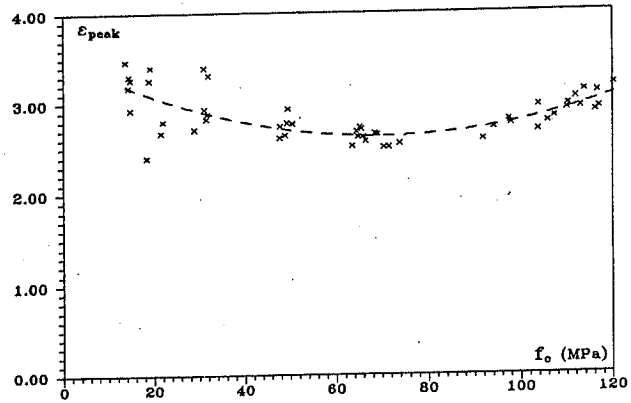

Fig. 6.3: Strain at peak stress, as a function of the uniaxial concrete strength.

It is seen that the peak strain has an apparent minimum at a concrete strength about 60 MPa. It is also seen that the scatter of the test results increases when the concrete strength falls below ~60 MPa. The scatter in the results from the lower strength concretes can be ascribed mostly to fact that the stress-strain curve for these concretes does not have a well defined peak. For concretes with a strength below ~30 MPa the stress-strain curves are very flat, and almost without curvature for strains in the region 2-4‰, see also appendix 1. This makes it hard to determine the peak strain. The influence of noise or false readings from the measuring devices will also increase, when the curve is almost without curvature, thus increasing the apparent scatter of the test results.

In Fig. 6.4 the test results are compared to various experimental results from other investigators.

At a first glance it seems as if almost any conclusion can be drawn from these results. However, inspecting the individual test series leads to the conclusion that the peak strain has a tendency to be constant for normal strength concrete, and increase for high strength concrete. Furthermore there are 2 parameters which have not yet been included in the discussion. These parameters are the coarse aggregate type and the shape of the coarse aggregate.

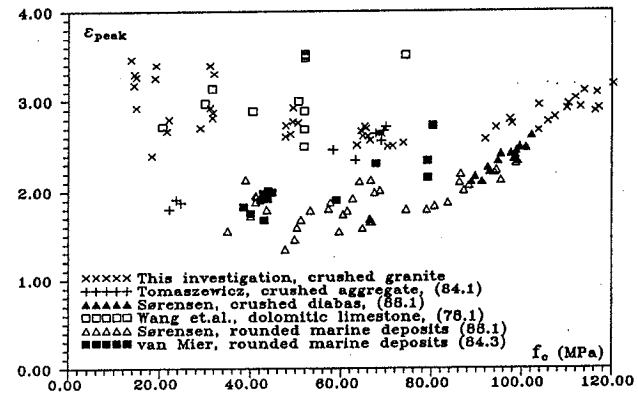

Fig. 6.4: Strain at peak stress, compared to various other investigations.

Consider first the aggregate type. It is known that different aggregates have different E-modulus, and different strengths. In rock mechanics the rocks are sometimes classified in terms of their modulus ratio, i.e. [68.1]. The modulus ratio is the E-modulus divided by the strength of the rock. Some rocks, such as granite and diabas, have a well defined modulus ratio, whereas other rocks, such as limestone have a much more varied modulus ratio. For the 3 rocks here mentioned, limestone generally has the highest modulus ratio followed by granite and diabas. Knowing the modulus ratio for a rock, it is possible to find a good approximation for the corresponding peak strain, se eq. (6.2).

$$\text{Modulus ratio} = \frac{E}{\sigma_{ult}} \quad \Rightarrow \quad \epsilon_{peak} \approx \frac{1}{\text{Modulus ratio}} \tag{6.2}$$

Consider now Fig. 6.4. It is seen that the test of Wang et.al. (limestone) shows a larger peak strain, than the test from this investigation (granite) which again shows a larger peak strain than the tests of Sørensen (diabas). It should now be evident that the peak strain is very much depending on the aggregate type.

These tests do not constitute irrefutable evidence because of the many differences and unknowns in the 3 test series. However, they point towards a new understanding of the problem.

Another parameter for the peak strain might be the shape of the coarse aggregate. Consider a crushed aggregate particle. Such a particle has a number of sharp protruding edges. When

the concrete specimen is loaded, a rather large stress field exists around any particle inside the concrete, see [88.1]. At the edges of the crushed aggregate particle these stresses will be intensified. The likelihood of microcracks emerging here at low stresses will therefore increase as compared to concretes using rounded coarse aggregate. These micro cracks will act as stress relievers for the larger cracks that later starts propagating, leading to failure. The effect of the increasing number of micro cracks will therefore be a softening of the stress-strain curve, and hereby an increase in the peak strain.

Comparing the test here presented to tests utilizing rounded marine deposits as coarse aggregate will support this theory. However, too many uncertainties makes it impossible to draw any definite conclusion.

One conclusion which can be drawn from the tests in this investigation, is that concrete using crushed granite aggregate seems to have a higher peak strain than concretes using rounded marine aggregate. This statement leads to eq. (6.3), which is an attempt to state the relationship between ϵ_{peak} and f_c for concretes with crushed granite aggregate. Eq. (6.3) incorporates the previously mentioned observations, that is constant value of the peak strain for most of the concrete range, and with a slight rise for the very high strength concretes. In determining this relation, some of the low strength concrete tests have been left out due to the difficulties in determining the peak strain, as described earlier. The relation follows the CEB-model, in that the peak strain is constant for a large range of concretes. For higher concrete strength the relation follows the trend from the test data, in that the peak strain increases when the concrete strength is increased.

$$\epsilon_{peak} = \begin{cases} 0.0027 & f_c \le 90 \text{ MPa} \\ 0.0027 + 0.0003 \cdot \dfrac{f_c - 90 \text{ MPa}}{30 \text{ MPa}} & f_c > 90 \text{ MPa} \end{cases} \tag{6.3}$$

In Fig. 6.5 are shown the test data compared to eq. (6.3). Also marked in Fig. 6.5 are the test results that have been disregarded when determining eq. (6.3). Eq. (6.3) are shown as the solid line. Also shown as a dashed line is the best fit curve for all of the test data.

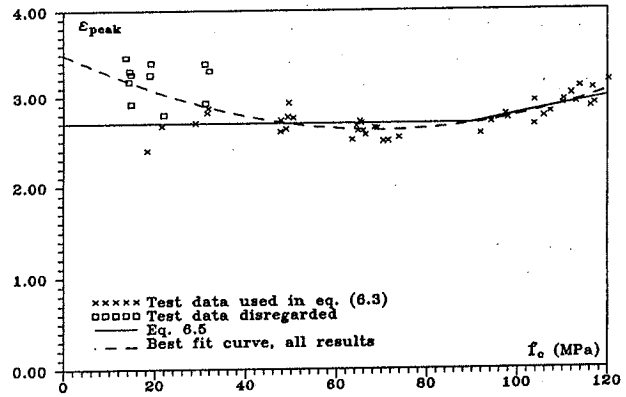

Fig. 6.5: Strain at peak stress, compared to eq. (6.3)

6.3 Concrete versus mortar

Concrete cylinders with a varying amount and size of the coarse aggregate have also been tested, as described in chapter 5. In Fig. 6.6 are shown the stress-strain curves for concrete E6, and the mortars M1 and M2.

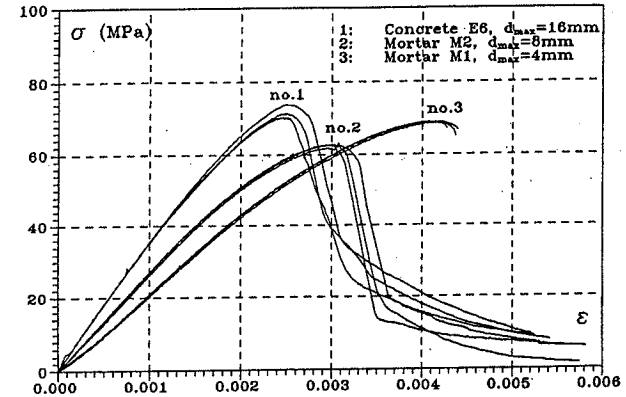

Fig. 6.6: Typical stress-strain curves for concrete and mortars.

Shown in Fig. 6.6 are 3 typical stress-strain curves from each of the casts. Referring to the description of the mix design for the 3 casts the following can be concluded.

- The strain at peak load is clearly depending on the size and amount of the aggregate used. Decreasing the size and amount of the aggregate will result in an increase in the peak strain.

- The E-moduli, E_{c0} and E_{c45}, are depending on, not only aggregate type and perhaps shape, as described in the previous chapter, but also on the size and amount of the aggregate.

- The descending part of the stress-strain curve is also depending on the size and amount of the aggregate used. It is seen that the slope of the descending part is increased for a decreasing aggregate size and amount. This is seen because the descending part can be captured by the test rig for the concrete E6. It can be observed in the tests of mortar M2 that the test rig does not quite have the necessary stiffness to capture all of the descending part of the stress-strain curve. This because the stress-strain curve here is linear. The linearity on the descending part is due to a large drop in the stress in the concrete between two recorded data signals. Finally in the case of the mortar M1 it can be seen that the test rig catches almost nothing of the descending part.

  Furthermore it can be seen that the aggregates will have a softening effect on the descending part. This partly because of the change in the slope of the descending part, but also because of the shape of the descending part. It is seen that increasing the aggregate size and amount will result in diminishing the stress drop after peak, and hereby increasing the area below the flat tail of the stress-strain curve.

The fact that the coarse aggregate plays an important part in the shape of the stress-strain curves is due to the differences in the material properties of the rock and the cement paste. These differences will create large stress variations around the aggregate particles. This lends a certain amount of validity to the theory of the influence of the aggregate shape on the peak strain, as described in chapter 6.2.

These conclusions also make it clear that comparing different test results is difficult, and great care should be taken.

6.4 Modelling the stress-strain curve

Choosing a model to evaluate test results against is not easy to do. In this case the CEB model has been chosen. The following arguments have been applied:

- The Exner model seems to give a good fit for the tail of the descending branch. However, at the rest of the stress-strain curve, the model is not within acceptable limits of the test results. Furthermore the model is not very easy to use, and the resulting stress-strain curve is very sensitive to changes in the parameters.

- Both the Tomaszewicz model and CEB model yield acceptable results. The resulting stress-strain curve from the Tomaszewicz model, however, has also proven to be rather sensitive to the parameters k and n.

- The CEB model is very easy to use.

Due to these arguments, and because the CEB model probably is the best known of the three models, it has been decided to use the CEB model for modelling the stress-strain curve.

In appendix 1 are shown the stress-strain curves for all of the tests performed. Also in these diagrams the modified CEB model have been drawn. The CEB model is modified in the following way:

- The E-modulus have been determined by using eq. (6.1), rather than using the original CEB formula for the E-modulus which is described in chapter 2. This is not done because a change in the formula for the E-modulus is needed, but in order to get a closer fit between the new model and the test results.

- The formula for the strain at peak load has been changed. It is clearly seen in chapter 6.2 that a constant value of 2.2‰ does not resemble the reported test data. This because the peak strain is depending on more than the concrete strength, i.e. aggregate type. Furthermore a change in the CEB model is needed, if the model is to be used for concrete with a strength of more than ~90 MPa. This because for the very high strength concretes the secant modulus, E_{peak}, will exceed the E-modulus at the origin, E_{c0}, when ϵ_{peak}=2.2‰ is used. The modelling of the peak strain, therefore, has to be changed. As a consequence eq. (6.3) has been used rather than the CEB value of 2.2‰.

Referring now to the stress-strain curves in appendix 1 the following can be observed:

- The modified CEB model exhibits an almost perfect match with all the experimental stress-strain curves for strains below the peak strain.

- For low strength concretes, $f_c \leq 20$ MPa, does the modified CEB model also present an almost perfect match on the descending part of the stress-strain curve, at least for strains below 6‰. This is perhaps not surprising, because the stress-strain curves for these concretes are very flat, and almost without curvature in the region $1.5‰ \leq \epsilon_c \leq 5‰$.

- For normal strength concretes, $20 \text{ MPa} < f_c \leq 50$ MPa, it can be seen that the descending part predicted by the modified CEB model does not quite follow the experimental stress-strain curves. The curve from the model descends a little too much, but the differences between the model and the experimental data are not excessive.

- For high strength concretes, $50 \text{ MPa} < f_c \leq 90$ MPa, does the modified CEB model also descend a little too much on the descending part of the stress-strain curve. The differences between the model and the experimental data are less than for the normal strength concretes. However, the modified model does not catch the rather small interval of strain where the experimental stress-strain curves change from being ascending to being descending. The result is a more slowly curving stress-strain curve than the experimental data suggest. The difference between the model and the experimental curves is mostly due to the overestimation of the peak strain which is experienced in this concrete strength interval when using eq. (6.3).

- For very high strength concretes, $f_c > 90$ MPa, is the model very close to the test data, except for the 'tail' of the stress-strain curve. Although most of the concrete specimens in this strength region exhibited partial failure, it seems that the model overestimates the large stress drop that occurs after peak stress. The problem, however, does not appear serious but merits further study.

The conclusion of this investigation is that the modified CEB model yields very good results when compared to the experimental stress-strain curves of this investigation. Due to this observation, and the observations mentioned previously in this chapter, it must therefore be concluded that future work needs to be centered around the prediction of the strain at peak stress. It seems clear that the peak strain is the reason for most of the deviations between the CEB model and the test results. It is also possible that the descending part of the models stress-strain curve needs to be changed a little. However, the difference between the model

and the experimental data does not warrant any major work in this area.

In Fig. 6.7 are shown stress-strain curves for varying concrete strength as predicted by the modified CEB model.

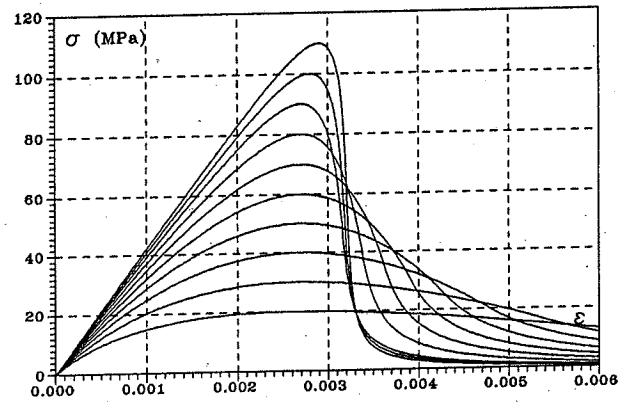

Fig. 6.7: Stress-strain curves for varying concrete strength, modified CEB-model.

6.5 Cracks in the concrete

In this chapter will the findings of the studies of the polished sections be given. The polished sections were studied partly with the naked eye, and partly using a microscope with a magnification of 40x. Using this technique, it is possible to see cracks with a crack width down to w=0.005 mm

Low strength concrete, pre-peak region

In the pre-peak region almost no cracks are found, Fig. A.2.1 - A.2.3. The few cracks that are visible are microcracks, that is $w<0.01$ mm. It was also observed that almost the same number of microcracks was found in the unloaded specimen, Fig. A.2.1, as in the loaded specimens, Fig. A.2.2 and A.2.3. Those very few microcracks found were either in the interface between the aggregate and the paste, or radiating from the aggregate particles. The microcracks must therefore be contributed to the shrinkage of the concrete specimens, rather than the loading.

High strength concrete, pre-peak region

In the unloaded specimen, Fig. A.2.12, some microcracks were found, $w<0.01$ mm. As the load is increased, Fig. A.2.13 and A.2.14, the number of microcracks also seems to increase. However, not very many microcracks were found in either of the specimens. All of the cracks have the same general appearance, that is most of them are radiating from the larger aggregates, and almost no cracks are found in the interface between the aggregate and the paste. Part of this crack system must therefore be due to shrinkage. Since the number of cracks seems to increase for increasing load, the loading must therefore also have contributed to the cracking.

Low strength concrete, peak load

In the low strength concrete almost no cracks were found at the peak load, Fig. A.2.4 and A.2.5. However in the center of the specimen some light areas are observed. These areas can be interpreted as follows: There have been some microcracks in this area. Due to the lack of coherent crack system these areas at the center were not injected with epoxy resign. Later at the sawing of the specimen the cement paste was not strong enough to withstand the load from the diamond saw, and they collapsed creating voids instead. Apart from these possible cracks, almost no microcracks and no larger cracks were found.

High strength concrete, peak load

Some microcracks were found in the high strength concrete specimen at peak load, Fig. A.2.15. These cracks have the general appearance as described in the pre-peak region. Also near the ends, some indications of fine cracks, $0.1>w>0.01$ mm were found. These cracks seem to have started at the corners and worked their way in. However again, not very many cracks were found.

Low strength concrete, post-peak region

In the post-peak region, Fig. A.2.6 - A.2.11, cracking of the low strength concrete increases. The cracks start forming larger and larger coherent crack systems. Almost all of the cracks run in the interface between the aggregate and the paste, and in almost no cases through the aggregate particles. The orientation of the cracks is roughly either vertical or in the Coulomb lines. However, due to the aggregate particles the cracks turn and twist around the particles. The cracks have a crack width, $w<0.2$ mm.

High strength concrete, post-peak region

In Fig. A.2.16 - A.2.21 are seen the cracks in the high strength concrete specimens. This crack system is very much different from the crack system in the low strength concrete. As soon as the peak load is passed, a large number of cracks start forming.

The major cracks run roughly in the Coulomb planes, that is from one corner to the opposite corner. These cracks have crack widths of more than 0.5 mm. In addition to these large cracks, a large number of smaller cracks start forming in the center third of the specimen. The number and the length of these secondary cracks increases for increasing load. The crack width, however, seems fairly constant between 0.01 and 0.2 mm. These finer cracks are all vertical, and run through both paste and aggregate.

Low strength concrete, summary of observations

- In the pre-peak region no cracks, other than a few microcracks, appear.
- At the peak load there is some evidence of microcracking in the center of the specimen.
- In the post-peak region larger cracks start forming. These cracks form a more coherent crack system, but still the crack width is less then ~ 0.2 mm.
- The orientation of the cracks in the post-peak region is roughly either vertical or in the Coulomb lines, but the cracks run in the interface between the aggregate and the paste causing the cracks to twist and turn.

High strength concrete, summary of observations

- In the pre-peak region some, but not many, microcracks start forming. The microcracks are mostly radiating from the aggregate particles.
- At peak load almost no finer cracks, $0.1 < w < 0.01$ mm, are visible.
- In the post-peak region larger cracks start forming along the Coulomb lines. Large crack widths are observed in these cracks.
- In addition to these large cracks, more and more finer cracks form in the center third of the specimen. The crack width in these cracks stays below ~ 0.2 mm, and the orientation is vertical through both paste and aggregate particles.

After comparing the observations from the low strength concrete with the observations from the high strength concrete, the following can be concluded.

Concrete does not crack before the peak load is reached. The few microcracks observed in the pre-peak region, are connected to the increasing load, but it does not seem as if they themselves lead to failure. The increasing number of microcracks supports somewhat the theory of the influence of the aggregate shape, as described previously in this chapter. However, concrete using rounded smooth aggregates has not been tested in this investigation, so a conclusion cannot be made on this subject.

The post-peak region is characterized by crack growth. Two sets of cracks have been observed: large cracks in the Coulomb lines, and smaller cracks in the center of the specimen. The large cracks seem to start at the surface and propagate towards the center, whereas the smaller cracks stay in the center where they increase in length and numbers, breaking up the material.

It seems clear that the shape of the stress-strain curve is closely related to the cracking of the concrete. The more brittle the material is, the more steeper the stress-strain curve is, and the more and the faster cracks appear.

What then happens prior to peak, when the stress-strain curve looses its initial liniarity and becomes more and more horizontal, is still an open question. This because, apparently the non liniarity is not associated with crack growth. One way of describing this behavior is to assume that yielding takes place in small parts of the specimen, i.e. in the Coulomb lines. This question, however, is not answered by this investigation, but is left open for other investigators.

Chapter 7

Conclusion

During this investigation it has been found that the aggregate has a large influence on the material properties of concrete. In all the areas where this investigation has been centered, the E-modulus, the strain at peak stress, and the descending part of the stress-strain curve, the influence of the aggregate has been rather large.

It has also been shown that the strain at peak stress merits further work. This especially in view of the much criticized brittle failure of high strength concrete. If the parameters that influence the peak strain are better known, high strength concrete can be produced with a large peak strain. This may not influence the very abrupt failure of high strength concrete, although some investigators have reported stress-strain curves of high strength concretes with high peak strain and shallow descending part [78.1]. But at the very least it will present the observer with an early warning of impending failure, due to the increase in deformation of the high strength concrete member.

If the strain at peak load can be determined, it has been found that the CEB model is in close agreement with the stress-strain curve up to a strain of $\epsilon_{c,max}$. The strain $\epsilon_{c,max}$ corresponds to $\sigma=0.5f_c$ on the descending part of the stress-strain curve. The remainder of the stress-strain curve can be approximated by the CEB model, however more work is needed in modelling the last part of the stress-strain curve.

The polished sections have given new knowledge concerning cracking and crack growth in concrete. It has been found that cracking of concrete mainly takes place after peak load has been reached, that is, on the descending part of the stress-strain curve. What then determines the peak load is still not fully understood. However, it should be clear that the descending part of the stress-strain curve not only is, what sometimes is called a structural response, but very much also a material response which is depending on the composition and strength of the concrete considered.

References

[64.1] ***The Testing of Brittle Materials Under Uniform Uniaxial Compressive Stresses.***
K. Newman and L. Lahance, ASTM Proceedings, vol 64, 1964, pp. 1044-1067.

[68.1] ***Rock Mechanics in Engineering Practice.***
K. G. Stagg and O.C. Zienkiewicz, John Wiley & Sons, 1968, pp. 4-12.

[78.1] ***Stress-Strain Curves of Normal and Lightweight Concrete in Compression.***
P. T. Wang, S. P. Shah & A. E. Naaman, Journal of the ACI, November 1978, vol 75, pp. 603-611.

[83.1] ***Betonbjælkers bøjningsbæreevne.***
H. Exner, ABK rapport R176, 1983.

[84.1] ***Betongens Arbeidsdiagram.***
A. Tomaszewicz, FCB/SINTEF rapport STF65 A84065, 1984.

[84.2] ***DS423 Betonprøvning.***
Dansk Standart 1984.

[84.3] ***Strain-Softening of Concrete under Multiaxial Loading Conditions.***
J. G. M. van Mier, Doctoral thesis, Eindhoven, Holland, 1984.

[88.1] ***Højstyrkebetons Deformationsforhold.***
M. B. Sørensen, M.Sc. thesis, ABK/LBM, DTH, Denmark 1988.

[90.1] ***CEB model code 90.***
Comite Euro-International du Beton, Bulletin d'information no. 203, 1991.

Appendix 1

Uniaxial stress-strain curves

In this appendix are presented all the uniaxial stress strain curves found in the investigation. Included in the graphs for the concretes E1-E9 are the stress-strain curves given by the CEB-model. In these curves the CEB-model has been altered in order for the E-modulus and the strain at peak load to conform to the actual test data.

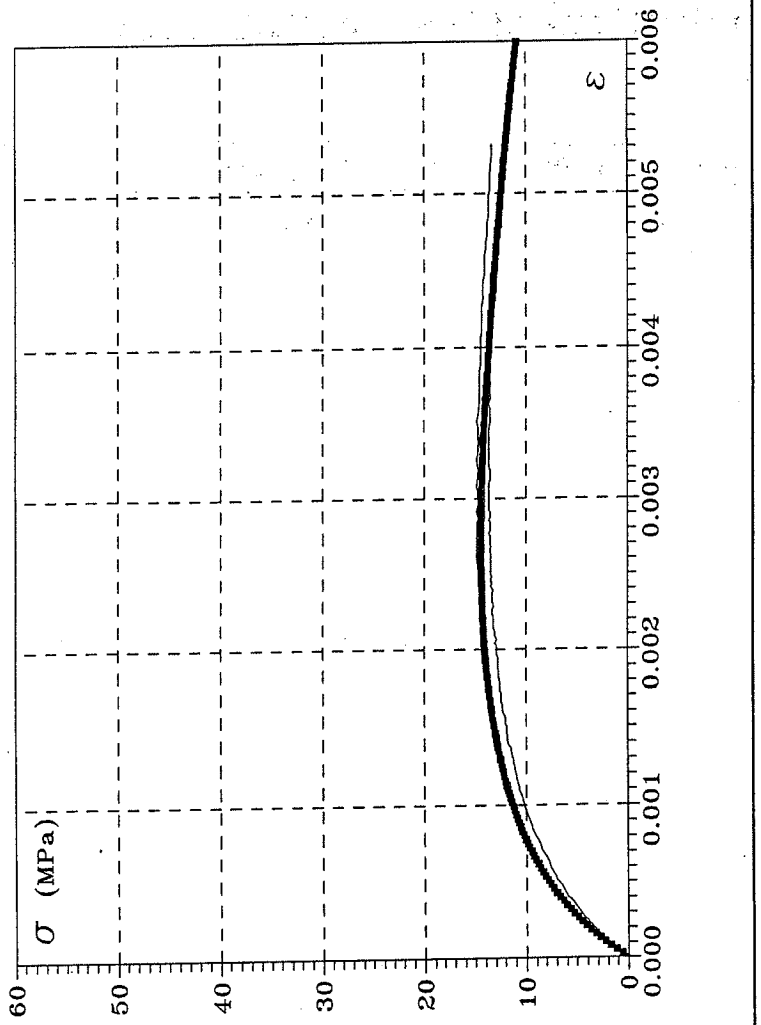

Fig. A.1.1: Uniaxial stress-strain curve for concrete E1. Thick line represents CEB-model.

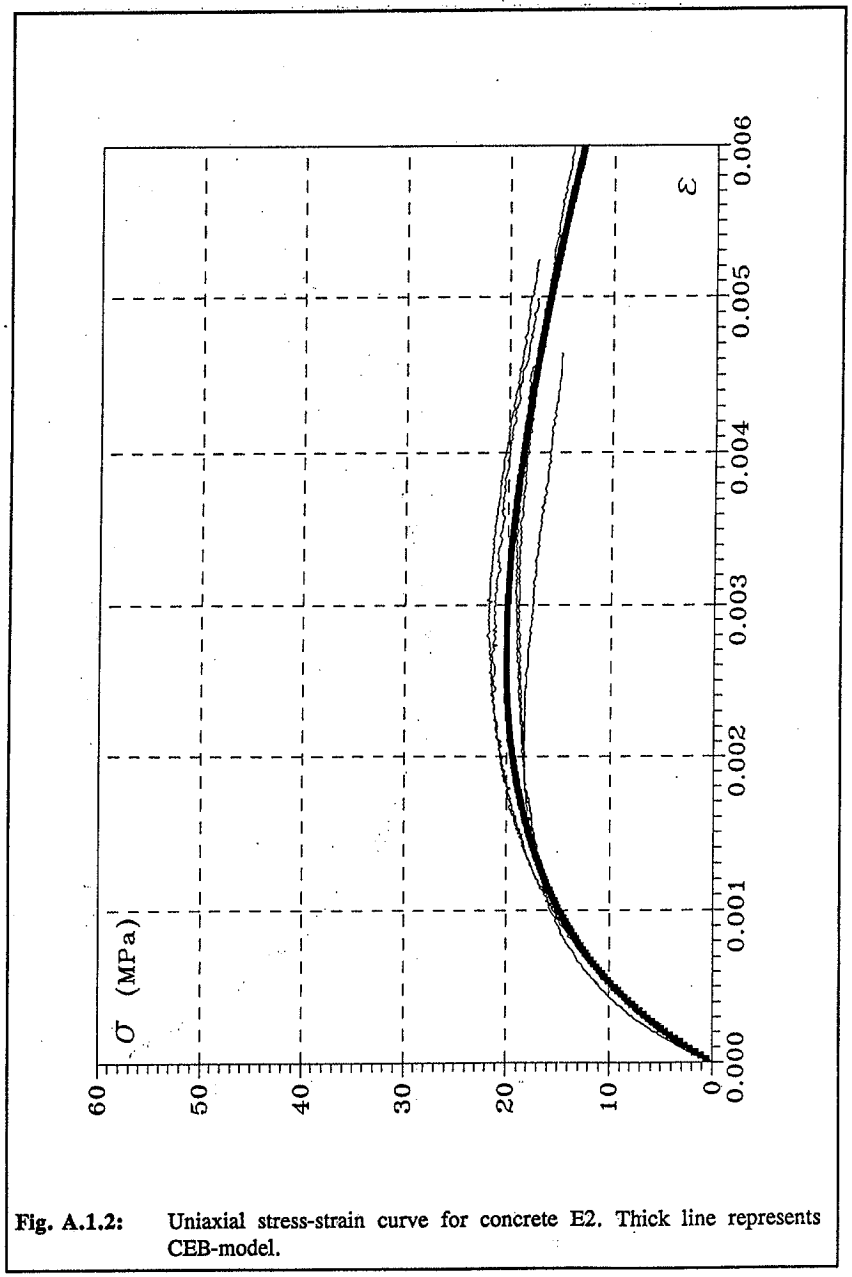

Fig. A.1.2: Uniaxial stress-strain curve for concrete E2. Thick line represents CEB-model.

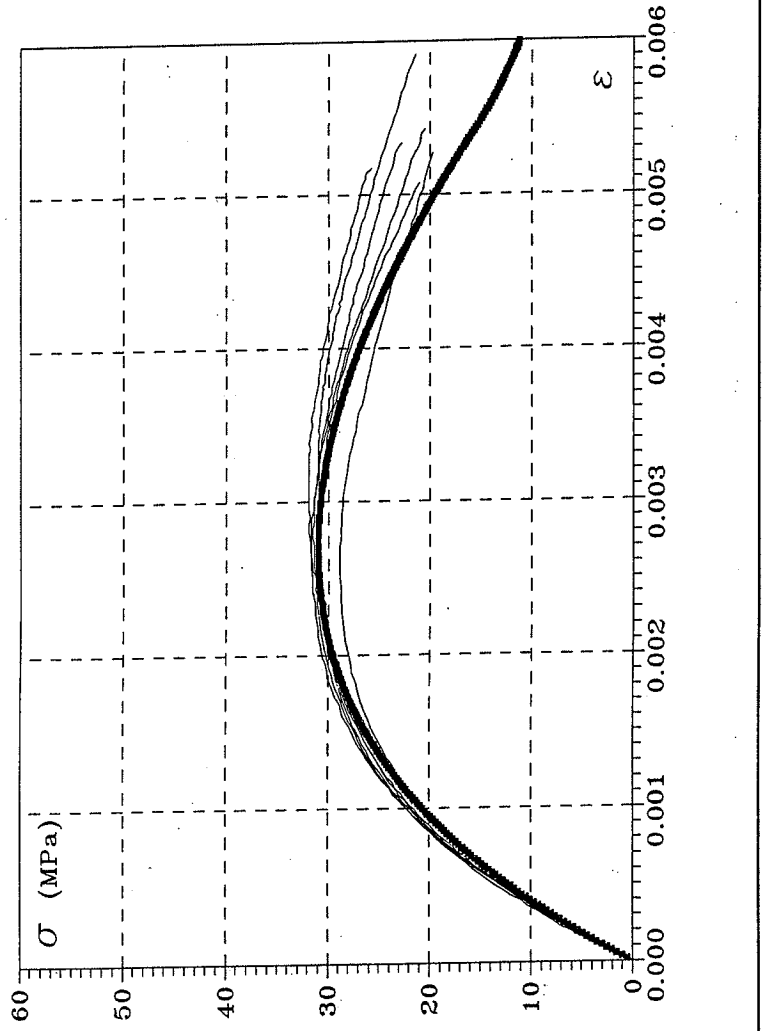

Fig. A.1.3: Uniaxial stress-strain curve for concrete E3. Thick line represents CEB-model.

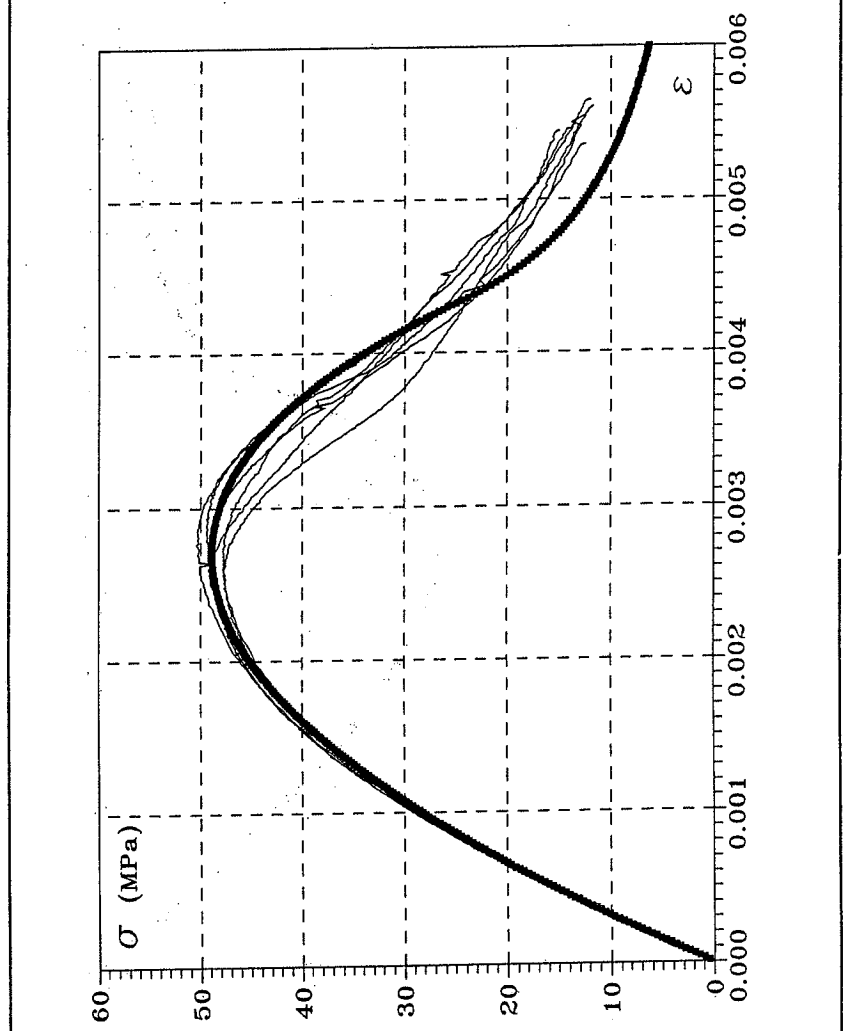

Fig. A.1.4: Uniaxial stress-strain curve for concrete E4. Thick line represents CEB-model.

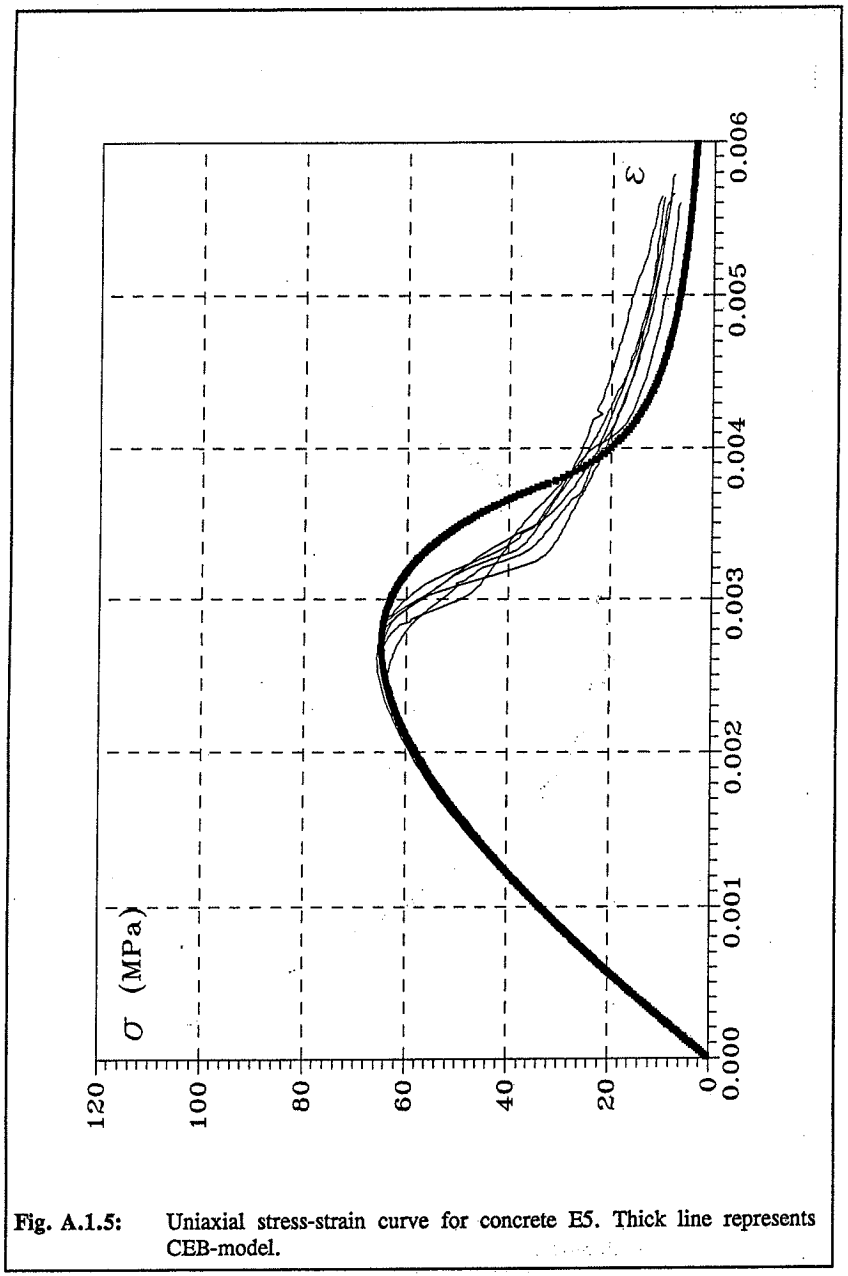

Fig. A.1.5: Uniaxial stress-strain curve for concrete E5. Thick line represents CEB-model.

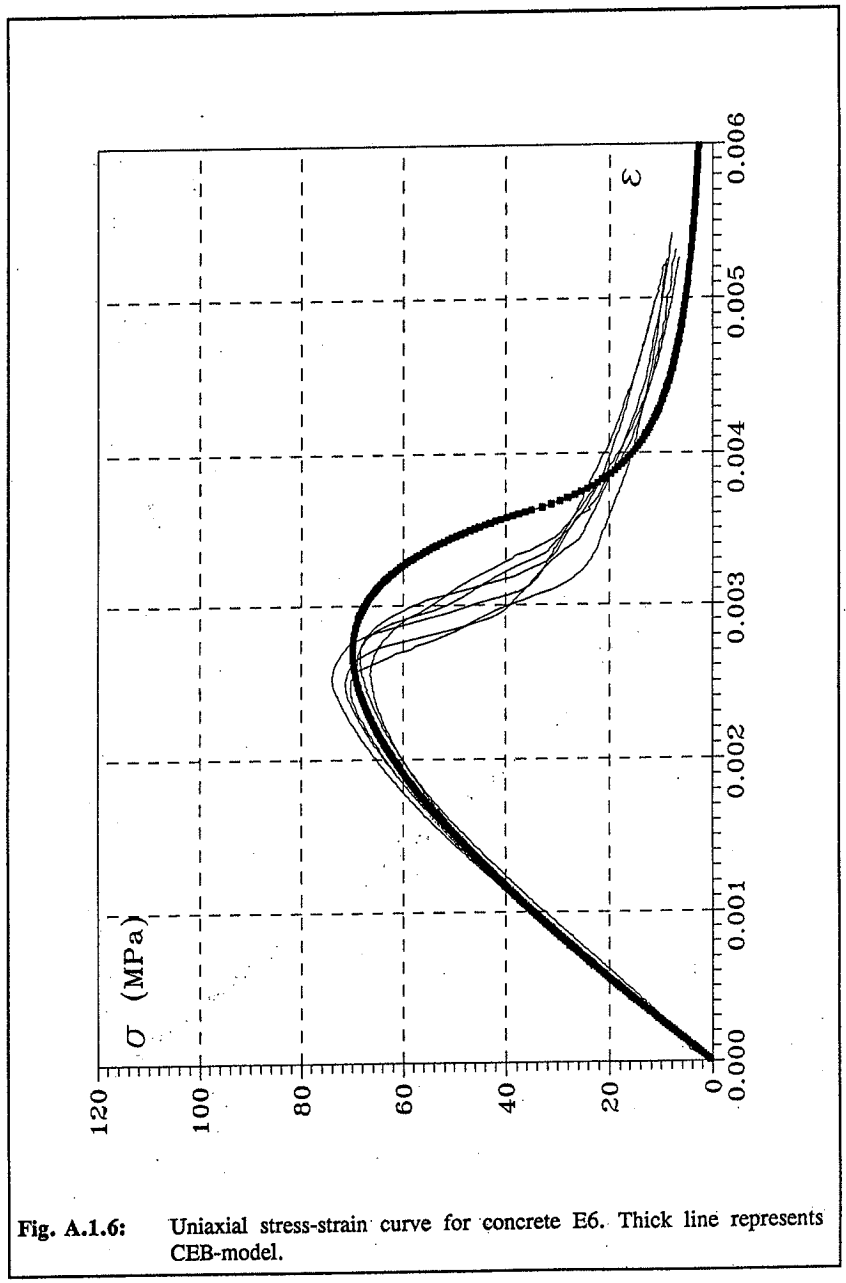

Fig. A.1.6: Uniaxial stress-strain curve for concrete E6. Thick line represents CEB-model.

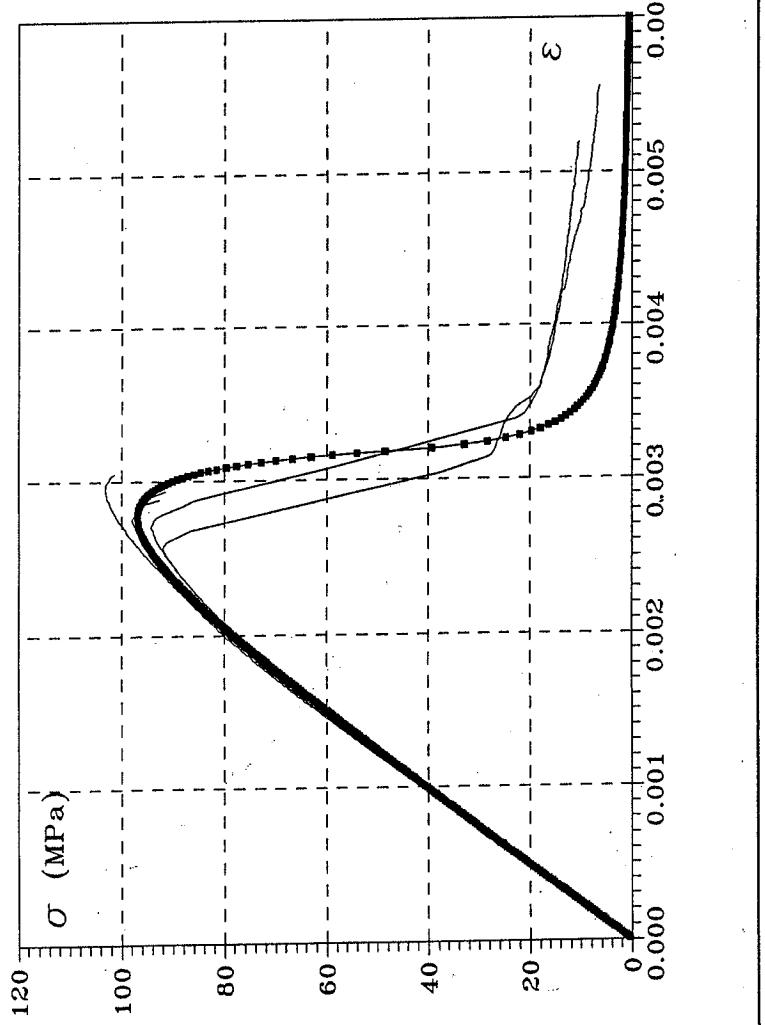

Fig. A.1.7: Uniaxial stress-strain curve for concrete E7. Thick line represents CEB-model.

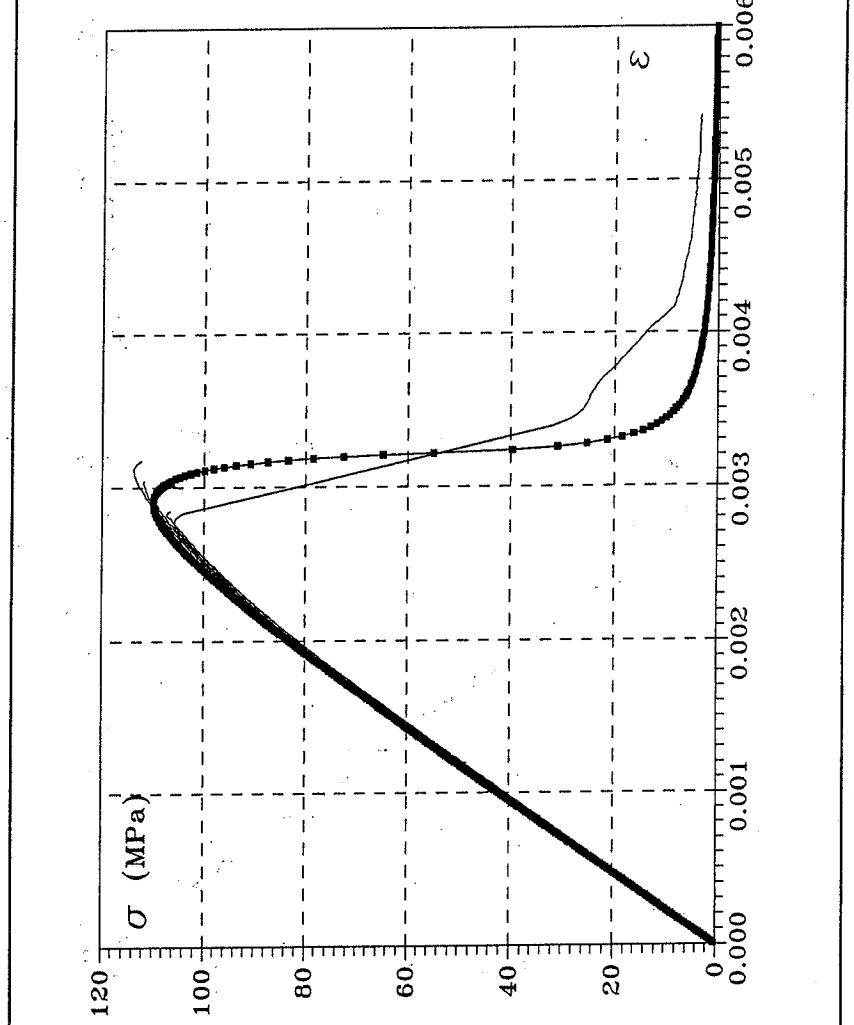

Fig. A.1.8: Uniaxial stress-strain curve for concrete E8. Thick line represents CEB-model.

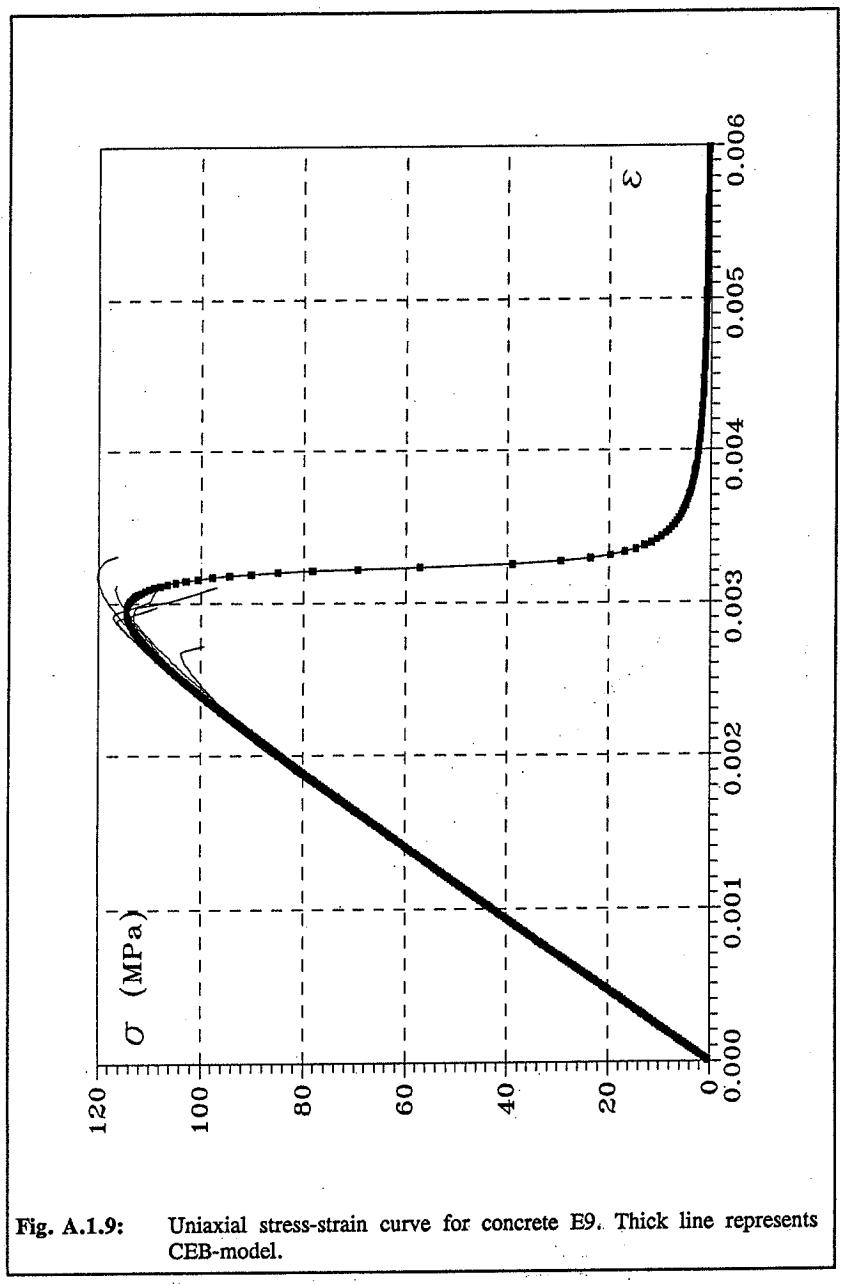

Fig. A.1.9: Uniaxial stress-strain curve for concrete E9. Thick line represents CEB-model.

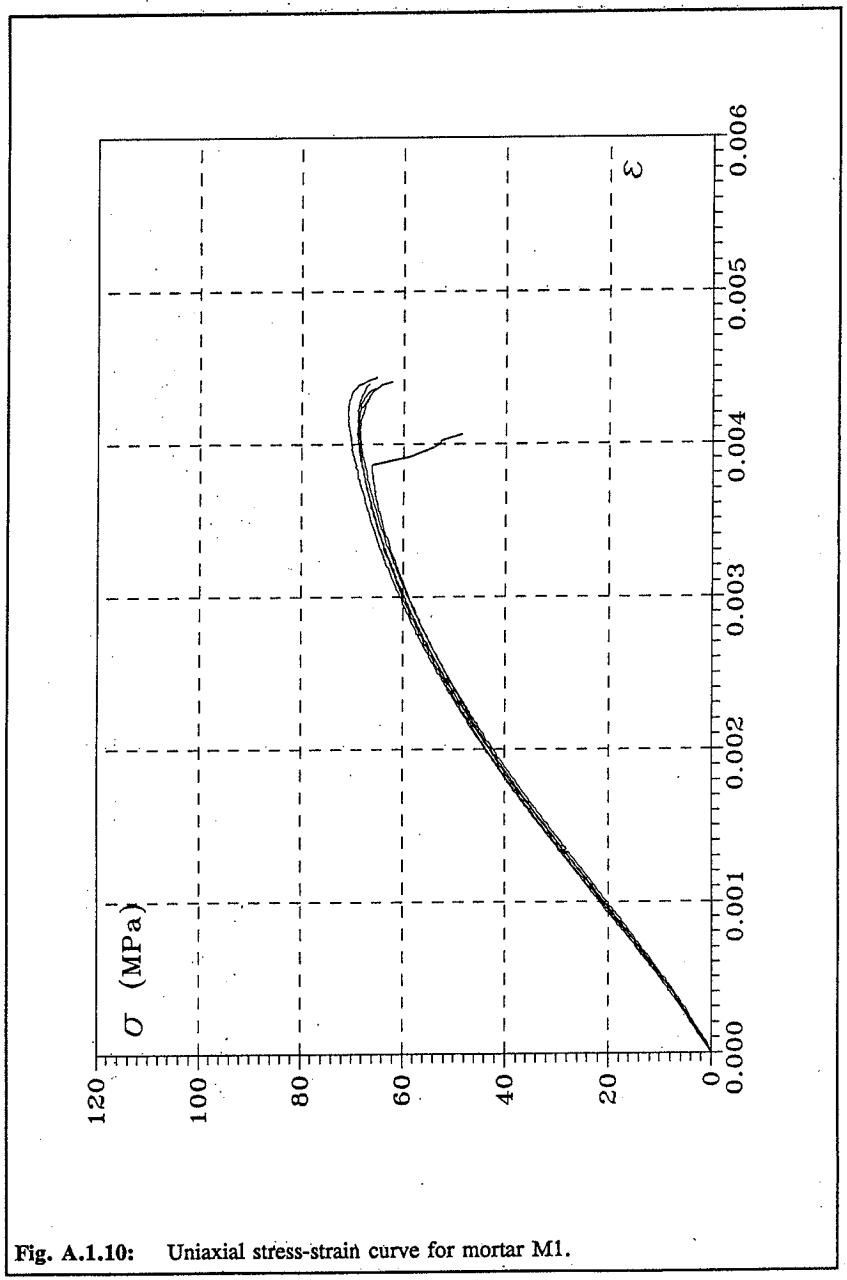

Fig. A.1.10: Uniaxial stress-strain curve for mortar M1.

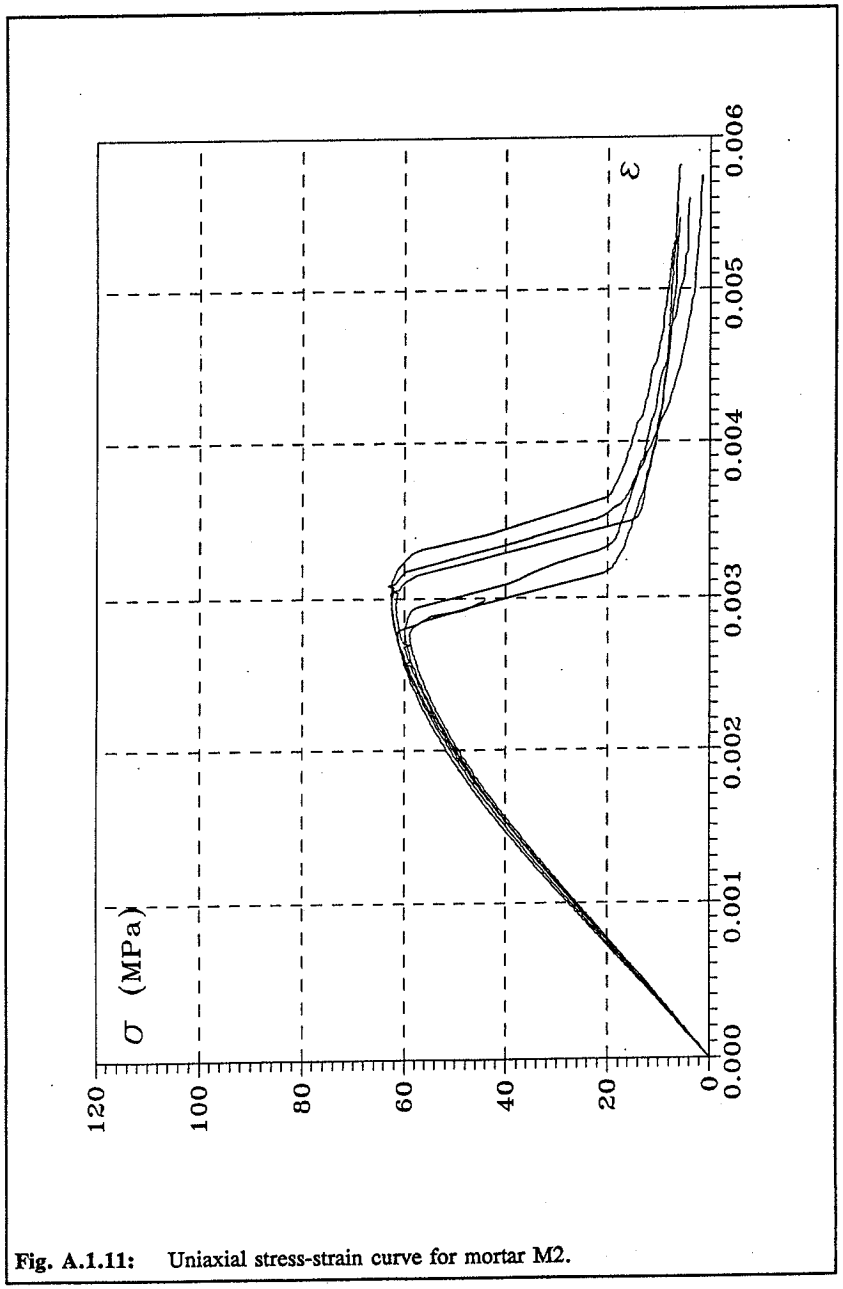

Fig. A.1.11: Uniaxial stress-strain curve for mortar M2.

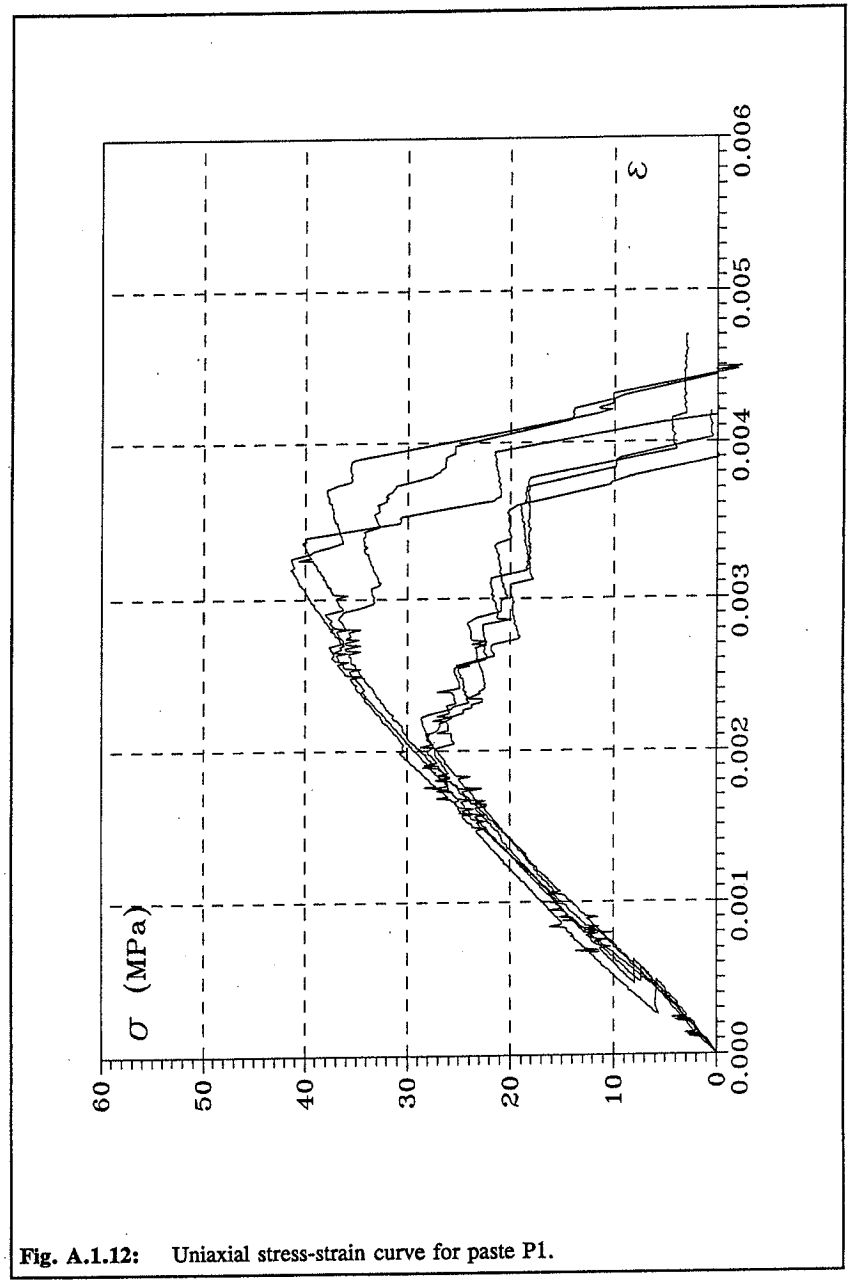

Fig. A.1.12: Uniaxial stress-strain curve for paste P1.

Appendix 2

Photographs of crack systems at various concrete strains

In this appendix are presented the photographs of the polished sections used for studying the crack systems and the crack propagation.

In the photographs, the light areas are the cracks and pores, the darker areas are the mortar, and the darkest areas are the aggregates.

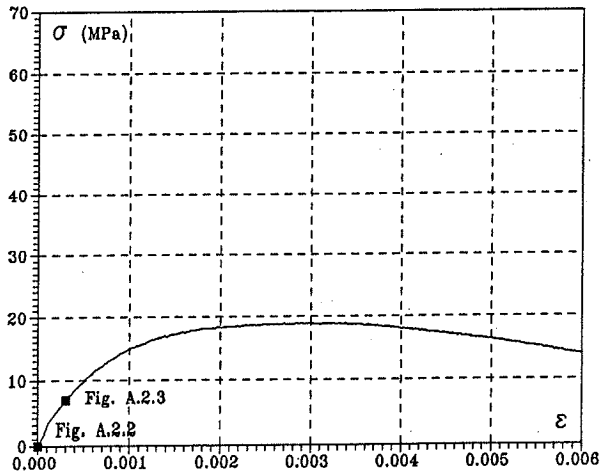

Fig. A.2.1: Placement of polished sections.

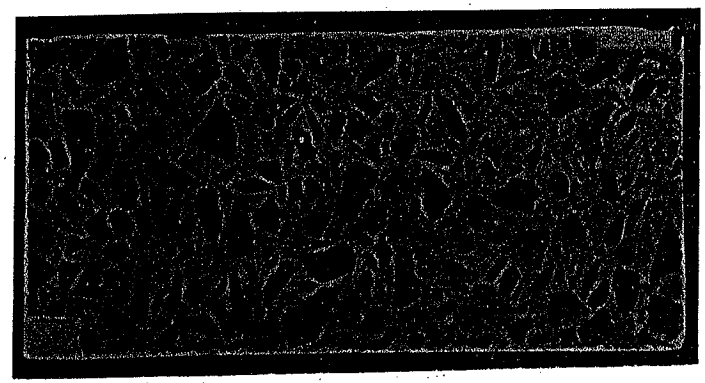

Fig. A.2.2: Low strength concrete, E2, unloaded.

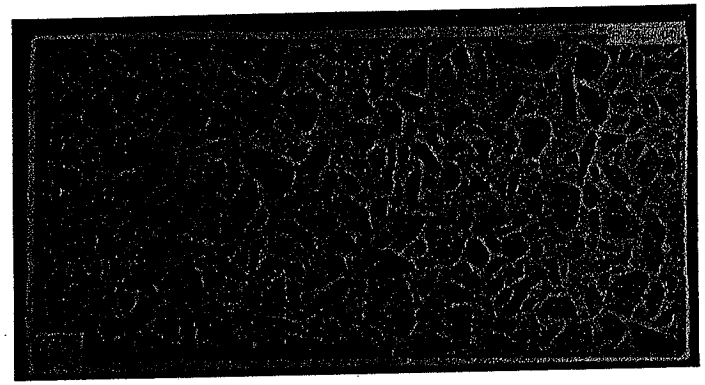

Fig. A.2.3: Low strength concrete, E2, at $\sigma=1/3f_c$.

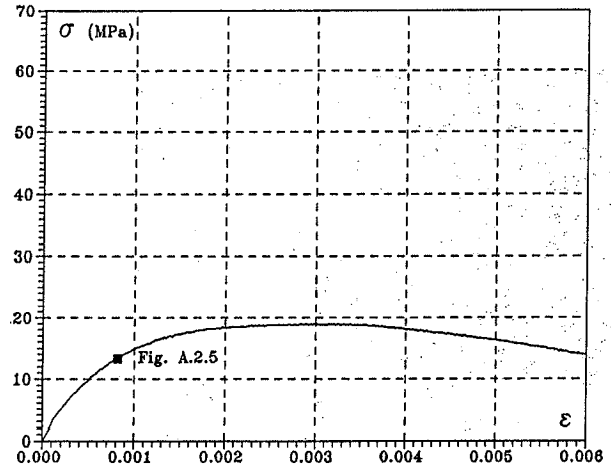

Fig. A.2.4: Placement of polished sections.

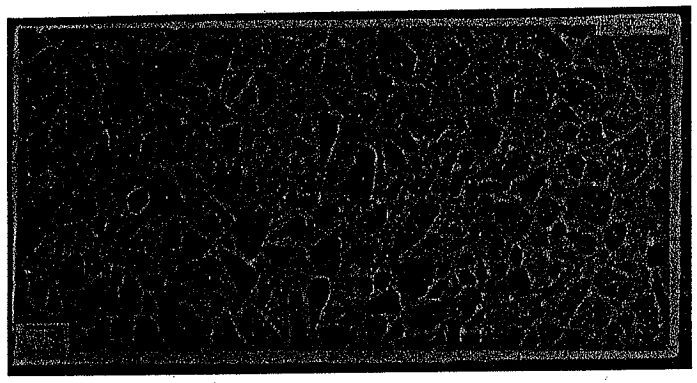

Fig. A.2.5: Low strength concrete, E2, at $\sigma=2/3f_c$.

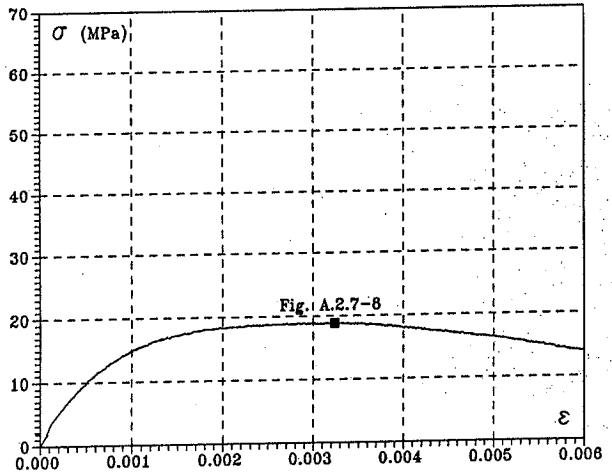

Fig. A.2.6: Placement of polished sections.

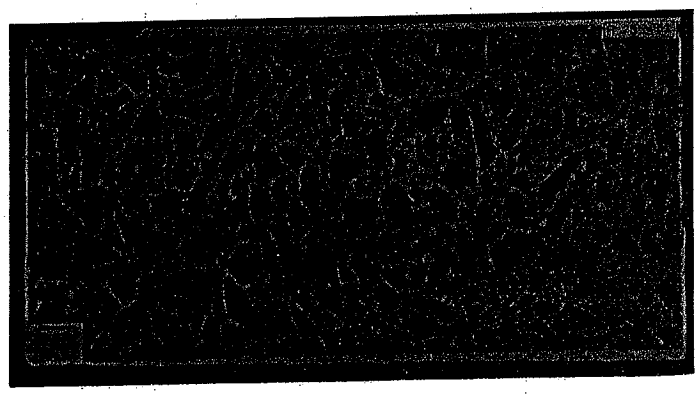

Fig. A.2.7: Low strength concrete, E2, $\sigma=f_c$.

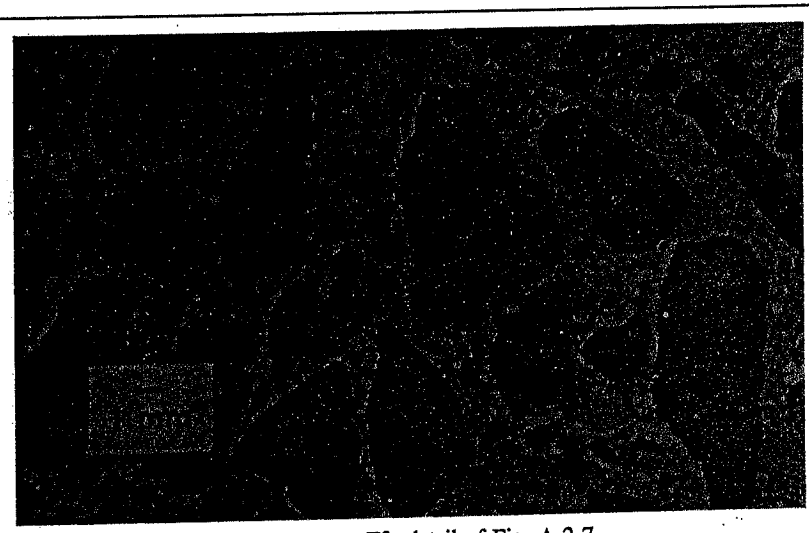

Fig. A.2.8: Low strength concrete, E2, detail of Fig. A.2.7.

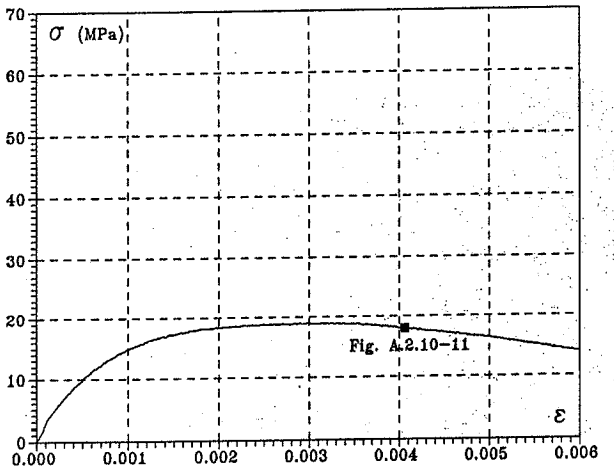

Fig. A.2.9: Placement of polished sections.

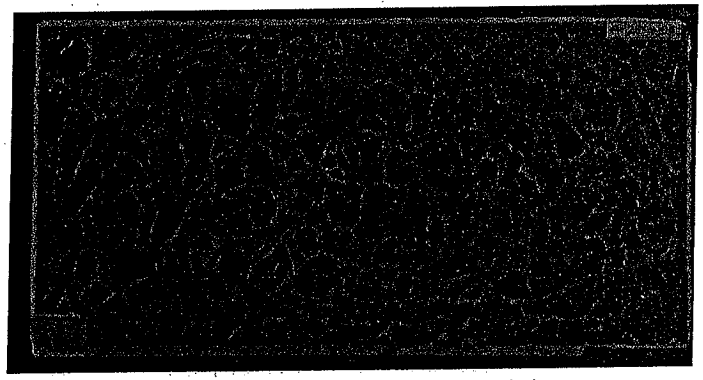

Fig. A.2.10: Low strength concrete, E2, at $\sigma = f_c - 1/3(f_c - \sigma_{0.006})$.

Fig. A.2.11: Low strength concrete, E2, detail of Fig. A.2.10.

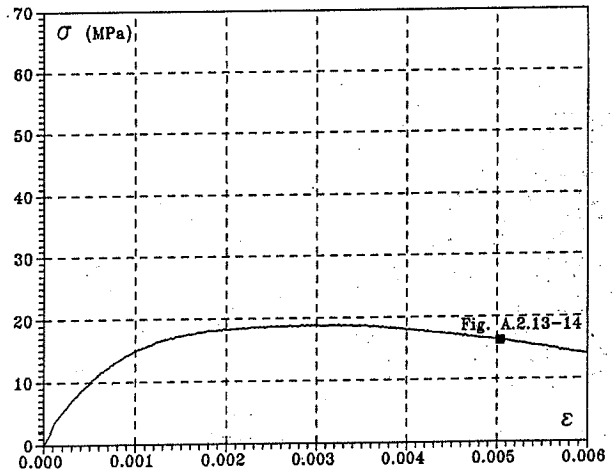

Fig. A.2.12: Placement of polished sections.

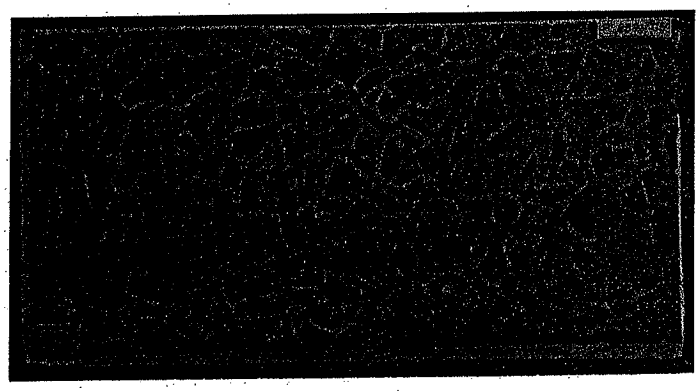

Fig. A.2.13: Low strength concrete, E2, at $\sigma = f_c - 2/3(f_c - \sigma_{0.006})$.

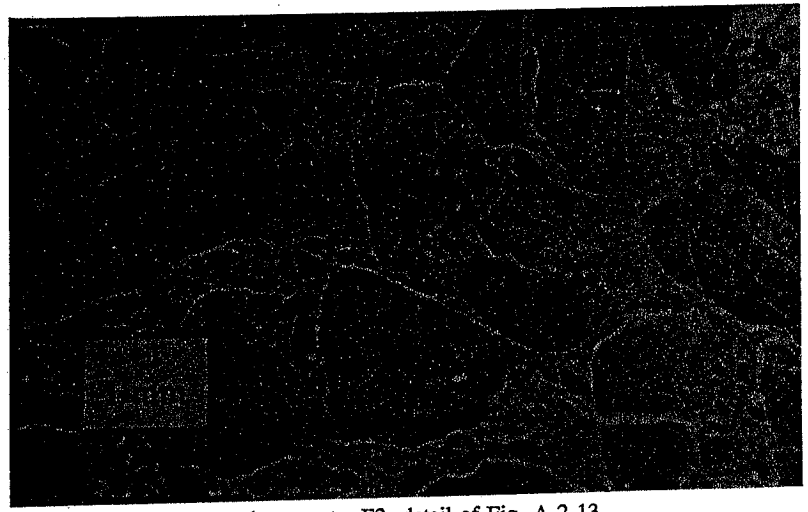

Fig. A.2.14: Low strength concrete, E2, detail of Fig. A.2.13.

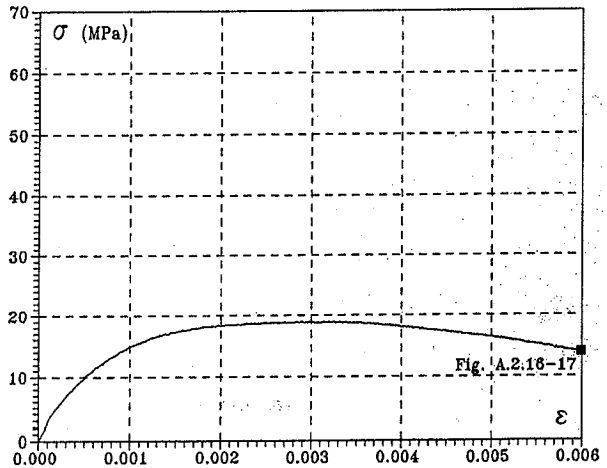

Fig. A.2.15: Placement of polished sections.

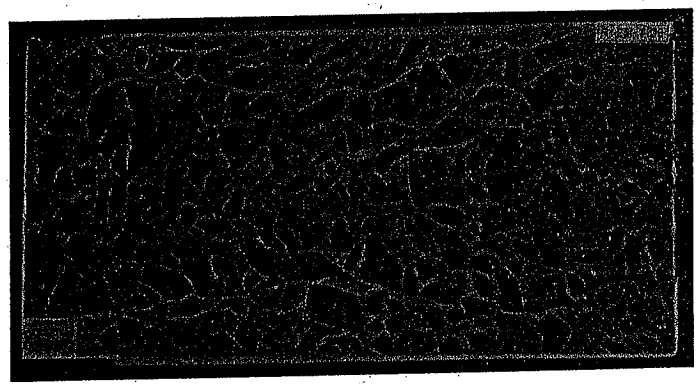

Fig. A.2.16: Low strength concrete, E2, at $\sigma = f_c - 3/3(f_c - \sigma_{0.006})$.

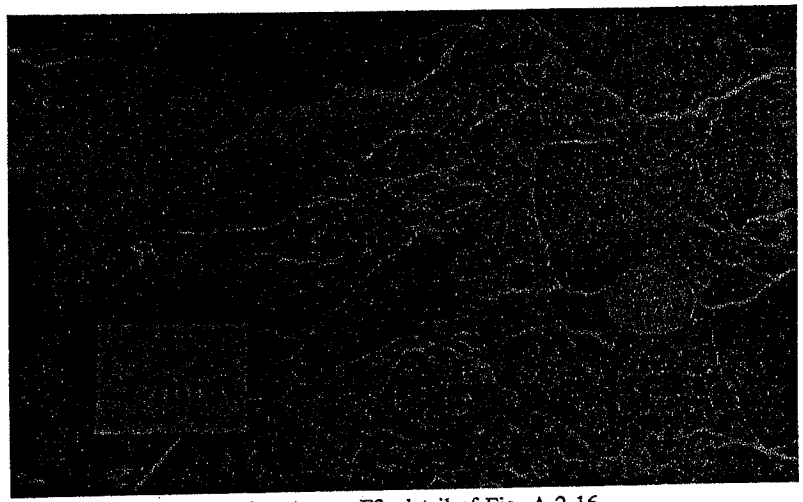

Fig. A.2.17: Low strength concrete, E2, detail of Fig. A.2.16.

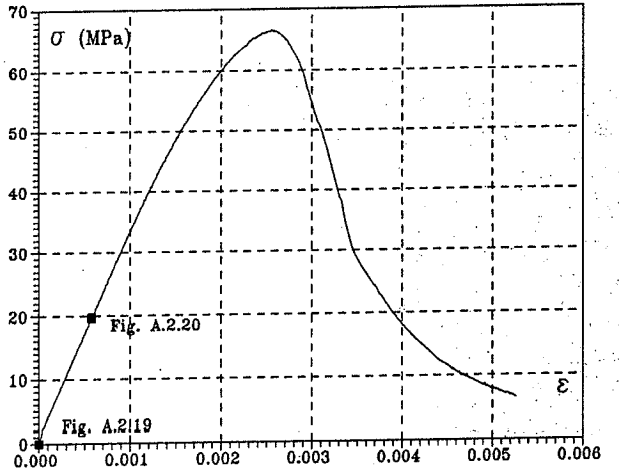

Fig. A.2.18: Placement of polished sections.

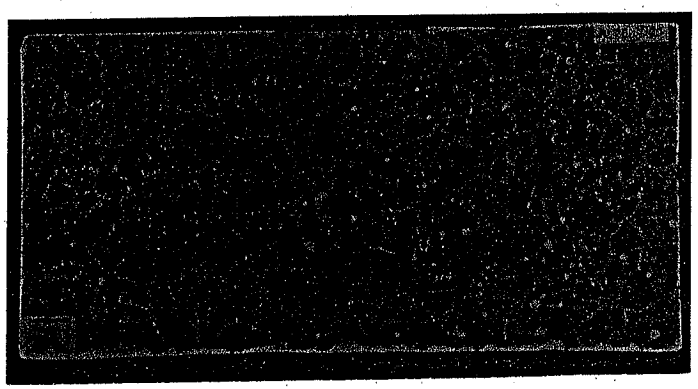

Fig. A.2.19: High strength concrete, E6, unloaded.

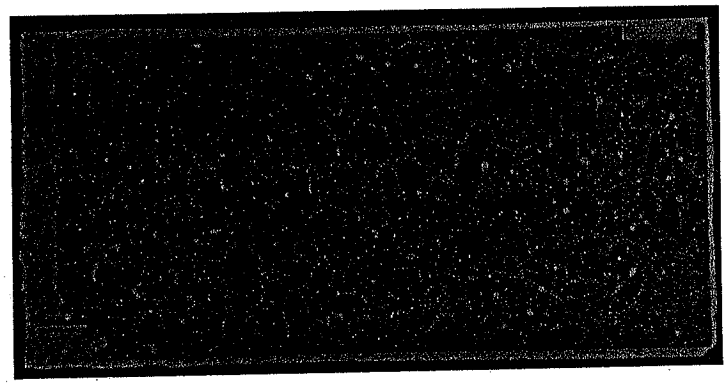

Fig. A.2.20: High strength concrete, E6, at $\sigma=1/3f_c$.

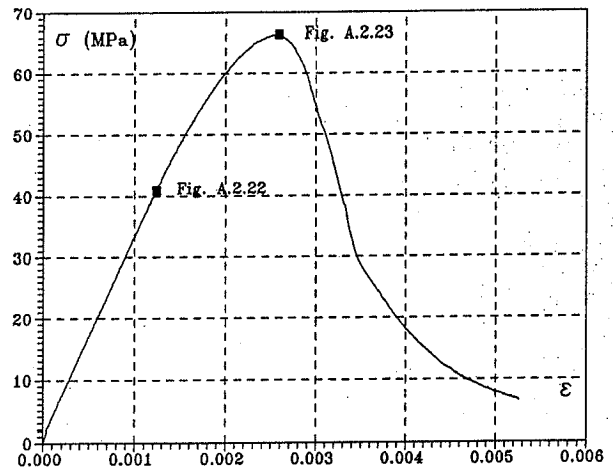

Fig. A.2.21: Placement of polished sections.

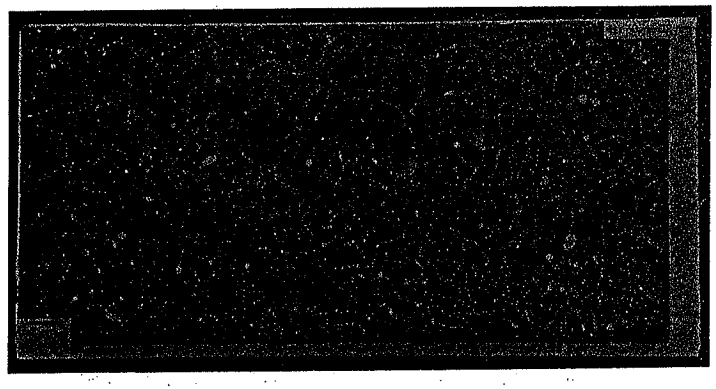

Fig. A.2.22: High strength concrete, E6, at $\sigma=2/3f_c$.

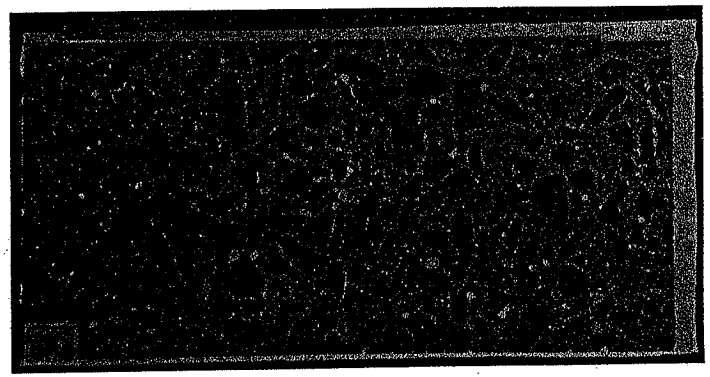

Fig. A.2.23: High strength concrete, E6, $\sigma=f_c$.

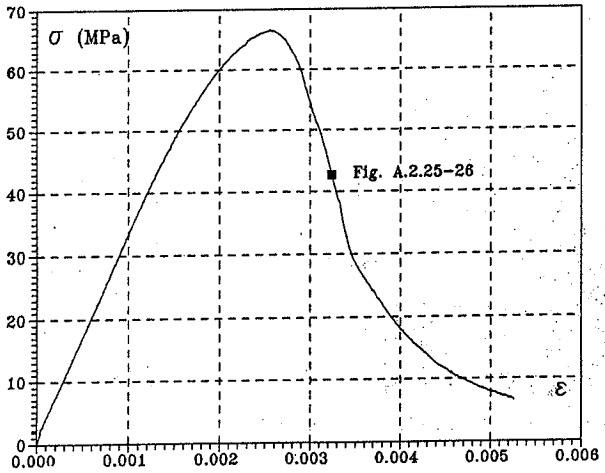

Fig. A.2.24: Placement of polished sections.

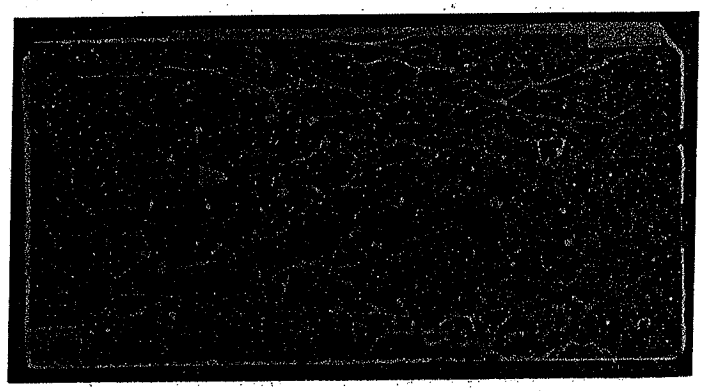

Fig. A.2.25: High strength concrete, E6, at $\sigma=f_c-1/3(f_c-\sigma_{0.006})$.

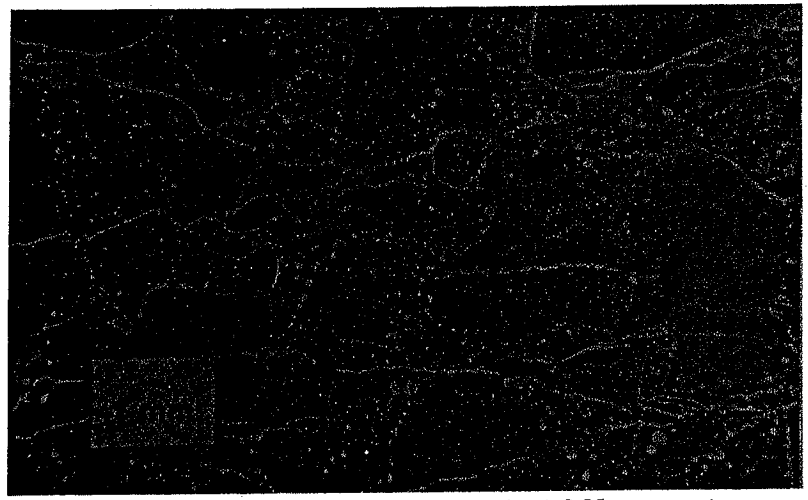

Fig. A.2.26: High strength concrete, E6, detail of Fig. A.2.25.

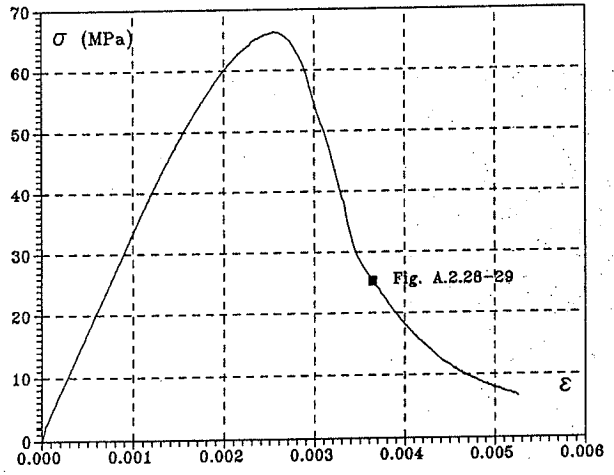

Fig. A.2.27: Placement of polished sections.

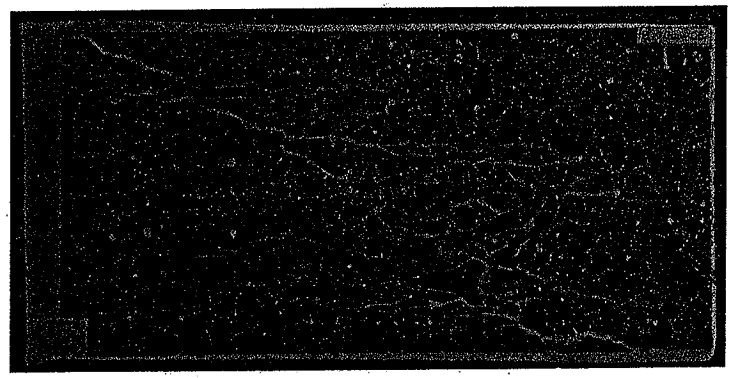

Fig. A.2.28: High strength concrete, E6, at $\sigma=f_c-2/3(f_c-\sigma_{0.006})$.

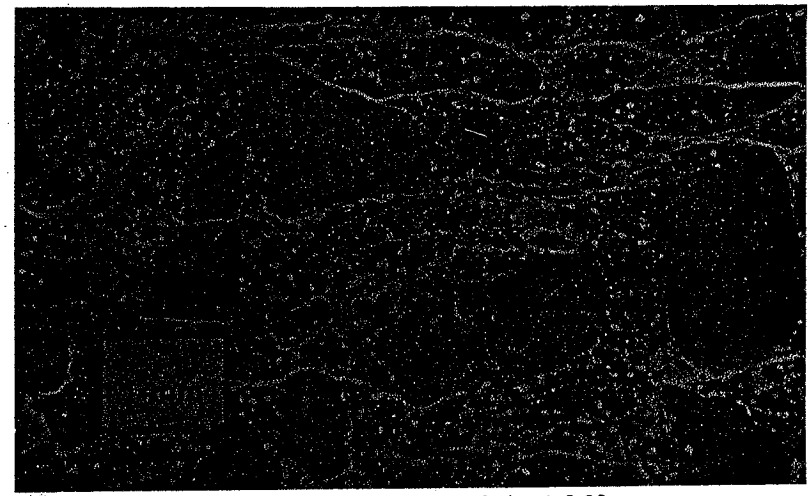

Fig. A.2.29: High strength concrete, E6, detail of Fig. A.2.28.

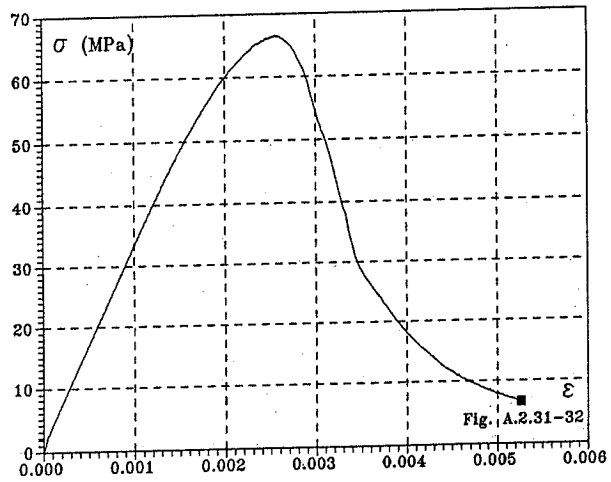

Fig. A.2.30: Placement of polished sections.

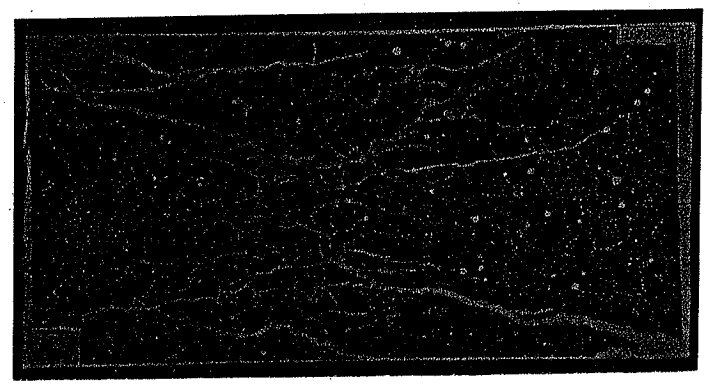

Fig. A.2.31: High strength concrete, E6, at $\sigma=f_c-3/3(f_c-\sigma_{0.006})$.

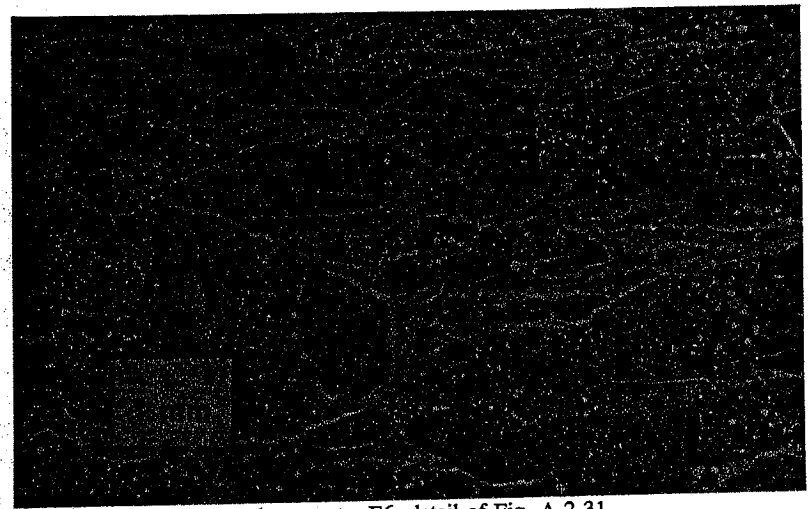

Fig. A.2.32: High strength concrete, E6, detail of Fig. A.2.31.